Impact of the Atlantic Warm Pool on the Summer Climate of the Western Hemisphere

Chunzai Wang[1]
Sang-ki Lee[2]
David B. Enfield[1]

[1] Physical Oceanography Division
NOAA Atlantic Oceanographic and Meteorological Laboratory
Miami, Florida

[2] Cooperative Institute for Marine and Atmospheric Studies
University of Miami
Miami, Florida

Revised to *Journal of Climate*

January 2007

Corresponding author address: Dr. Chunzai Wang, NOAA/AOML, Physical Oceanography Division, 4301 Rickenbacker Causeway, Miami, FL 33149. E-mail: Chunzai.Wang@noaa.gov.

Abstract

The Atlantic Warm Pool (AWP) is a large body of warm water comprised of the Gulf of Mexico, the Caribbean Sea, and the western tropical North Atlantic. Located to its northeastern side is the North Atlantic Subtropical High (NASH) that produces the tropical easterly trade winds. The easterly trade winds carry moisture from the tropical North Atlantic into the Caribbean Sea where the flow intensifies forming the Caribbean Low-Level Jet (CLLJ). The CLLJ then splits into two branches: One turning northward and connecting with the Great Plains Low-Level Jet (GPLLJ), and the other continuing westward across Central America into the eastern North Pacific. The easterly CLLJ and its westward moisture transport are maximized in the summer and winter, whereas they are minimized in the fall and spring. This semi-annual feature results from the semi-annual variation of sea level pressure in the Caribbean region owing to the westward extension and eastward retreat of the NASH.

The NCAR community atmospheric model and observational data are used to investigate the impact of the annual AWP on the summer climate of the Western Hemisphere. Two groups of the model ensemble runs with and without the AWP are performed and compared. The model results show that the effect of the annual AWP is to weaken the summertime NASH, especially at its southwestern edge. The AWP also strengthens the summertime continental low over the North American monsoon region. In response to these pressure changes, the CLLJ and its moisture transport are weakened, but its semi-annual feature does not disappear. The weakening of the easterly CLLJ increases (decreases) moisture convergence to its upstream (downstream), and thus enhances (suppresses) rainfall in the Caribbean Sea (in the far eastern Pacific west of Central America). Our model runs show that the AWP's effect is to always weaken the southerly GPLLJ. However, the AWP strengthens the GPLLJ's northward moisture transport in the summer because the AWP-induced increase of specific humidity overcomes the weakening of southerly wind, and *vice versa* in the fall. Finally, the annual AWP largely reduces the tropospheric vertical wind shear in the main development region that favors hurricane formation and development during August-October.

1. Introduction

Climate fluctuations in the Western Hemisphere have been largely attributed to well-known phenomena such as the El Niño-Southern Oscillation (ENSO), the North Atlantic Oscillation (NAO), the tropical Atlantic meridional gradient variability, and the Atlantic Niño. The importance of variability of the tropical Western Hemisphere Warm Pool (WHWP) has recently been pointed out (Wang and Enfield 2001 and 2003; Wang et al. 2006). At various stages of development, the WHWP is comprised of the eastern North Pacific west of Central America, the Gulf of Mexico, the Caribbean Sea, and the western tropical North Atlantic. Unlike the Indo-Pacific warm pool, which straddles the equator, the WHWP lies entirely north of the equator. Sandwiched between North and South Americas and between the tropical North Pacific and Atlantic Oceans, the WHWP is the second largest body of very warm water on Earth and hosts the second largest diabatic heating center in the summer tropics (summer shall always refer to the boreal season). The WHWP has a large seasonal cycle, and the interannual fluctuations of its area are comparable to the annual variation, as shown in Wang and Enfield (2001, 2003). The Central America landmass divides the WHWP into two ocean regions: The eastern North Pacific warm pool and the Atlantic Warm Pool (AWP) east of Central America.

Associated with the AWP is a maximum of easterly zonal wind (larger than 13 m/s) in the lower troposphere of the Caribbean (about 925-mb) during the summer, called the Caribbean Low-Level Jet (CLLJ) (Amador 1998; Amador and Magana 1999; Poveda and Mesa 1999; Mo et al. 2005; Wang 2007; Wang and Lee 2007). [Note that the CLLJ is referred to as "San Andres low-level jet" in Poveda and Mesa (1999).] As the CLLJ transits the Caribbean Sea, it is split into two branches: One turning northward and connecting with the Great Plains Low-Level Jet (GPLLJ), and the other continuing westward across Central America into the eastern North

Pacific. Since these jets in conjunction with the specific humidity serve to transport moisture for rainfall, it is expected that the AWP changes the jets' moisture transport and affects rainfall over the central United States and the eastern North Pacific. Additionally, tropical cyclones can be formed in the AWP or be intensified when they pass over the AWP. Thus, the AWP is an important region for both climate and hurricanes.

Using various data sets, Wang et al. (2006) show statistical evidence for the anomalous AWP influences on Western Hemisphere summer rainfall and Atlantic hurricanes. However, how and why (even whether or not) the annual (or normal) AWP affects the summer climate of the Western Hemisphere has not yet been shown. The purpose of this paper is to investigate and document the impact of the annual AWP on climate during the summer by using the NCAR community atmospheric model and observational data. The paper will show the influences of the annual AWP on the North Atlantic Subtropical High (NASH) and atmospheric circulations in the North Atlantic and over North America, and the annual variability of the CLLJ's moisture transport and its relations to rainfall. The paper will also demonstrate how and why the AWP is important for the Atlantic hurricane formation and development.

The paper is organized as follows. Section 2 describes the data sets and atmospheric model that are used in this paper. Section 3 shows the NASH and how it is affected by the AWP. Section 4 documents the variation of the CLLJ's westward moisture transport and its relationship to the AWP. Section 5 investigates how the AWP affects the GPLLJ. Section 6 examines summertime rainfall associated with the AWP. Finally, Section 7 provides a summary and discussion.

2. Data sets and model

Three data sets are used in this study. The first is the updated NCEP-NCAR reanalysis from January 1950 to December 2002 on a 2.5° latitude by 2.5° longitude grid (Kalnay et al. 1996). The second data set is precipitation product of the CPC (Climate Prediction Center) Merged Analysis of Precipitation (CMAP) (Xie and Arkin 1997). This data set blends satellite estimates and rain gauge data on a 2.5° latitude by 2.5° longitude grid available from January 1979 to the present. With these two data sets, we calculate monthly climatologies that are used to compare with model results. The third data set is climatological SST from Hadley Centre Sea Ice and SST data set (HadISST) on a 1° latitude by 1° longitude resolution (Rayner et al. 2003) which is used to force atmospheric model.

The atmospheric general circulation model used in this study is the latest version (version 3.1) of the NCAR Community Atmospheric Model (CAM3). The model is a global spectral model with a triangular spectral truncation of the spherical harmonics at zonal wave numbers 42 (T42), which roughly gives a 2.8° latitude by 2.8° longitude resolution. It is vertically divided into 26 hybrid sigma-pressure layers: The upper regions of the atmosphere are gridded by pressure while sigma coordinate system is used for the lower levels and a hybrid coordinate system is used in the middle layers. See Collins et al. (2006) for more detailed explanations about the physical parameterizations of CAM3, and Hurrell et al. (2006) for the model's performances for the seasonal variations and interannual variability.

We conduct two sets of ensemble simulations: Control (CTRL) and no AWP (NO_AWP) runs. In the CTRL run, the monthly HadISST climatological SST is prescribed globally for forcing the CAM3 model. Daily values of SST are obtained by linearly interpolating the monthly mean values. In the set of the NO_AWP simulations, we perform three model

experiments with different ways of removing the AWP to test whether or not the model results are robust. Three model experiments are designed to have different SST forcing only in the AWP region (from 5°N to 30°N between 40°W and the coast of the Americas), whereas outside the AWP (for the rest of the global ocean) all are forced by the monthly HadISST climatology. In the first one, the SST in the AWP box is held to its January value. In the second experiment, the SST within the AWP region cannot be larger than 26°C, i.e., the SST in the AWP box is set to 26°C if its value is larger than 26°C. In the third experiment, for a given month a uniform value is added at each grid point to keep the AWP box-averaged SST to that of January (24.96°C). To prevent discontinuity of SST forcing around the edges of the AWP box, a mask of weights is applied near the AWP boundary. The smoothing is applied to five model grids centered at the AWP boundary, with respective weights of 1.0, 0.75, 0.50, 0.25, and 0.0 from inside to outside model grids of the AWP boundary. All of three model experiments show a similar result, indicating that the model results are independent of how the warm pool is removed. In this paper, we present the second model experiment as the NO_AWP run. The SST forcing difference between the CTRL and NO_AWP runs in March, May, July, and September is shown in Fig. 1. It shows that the positive SST anomalies in the AWP region start in the spring, develop in the summer, and mature in the fall (around September).

For each set of simulations the model is integrated for 20 years. The first two years of output are discarded to exclude any possible transient spin up effects. A time mean is then calculated by averaging together the output for the remaining 18 years for each month or season. Assuming each year is statistically independent, this is equivalent to an ensemble mean with 18 members. To isolate the AWP's effect, the difference is taken between the runs with and without the AWP (CTRL minus NO_AWP).

3. North Atlantic Subtropical High (NASH)

The North Atlantic Subtropical High (NASH), centered over the eastern portion of the subtropical North Atlantic basin throughout the year, is a robust feature that affects directly the North Atlantic sector and its surrounding continents. The NASH is the most important factor in determining the strength of the trade winds (or low-level jets) and their associated surface evaporation, moisture transport, rainfall, and tropical cyclones. Thus, we first examine and discuss the model ensemble simulations of the NASH and the influence of the AWP on the NASH.

The horizontal structure of Sea Level Pressure (SLP) and the 925-mb wind vector during the summer (June-August; JJA) from both the NCEP-NCAR reanalysis and the CTRL run are shown in Figs. 2a and 2b. The CAM3 model does a reasonably good job in simulating the NASH although the modeled NASH is stronger and is centered farther eastward than the reanalysis. These model discrepancies in simulating the NASH's strength and position may affect other model simulated variables, as will be shown later. Both the reanalysis and model show that the NASH in the summer is in a cell-type configuration with a well-defined core region located in the eastern subtropical Atlantic Ocean where the ocean temperature is relatively cool. The high-pressure cell extends southwestward, reaching the western boundary of the North Atlantic Ocean basin. Figures 2a and 2b also show the North Pacific subtropical high that is stationed in the eastern North Pacific Ocean (Fig. 2 covers only part of the North Pacific subtropical high since our main focus is on the NASH). The simulated North Pacific subtropical high is also stronger than that of the reanalysis. Sandwiched between the NASH and the North Pacific subtropical high, North America has low pressure associated with the heated continent

during the summertime. At its southern and northern flanks, the NASH produces the easterly trade winds in the Tropics and the westerly winds in the mid-latitudes. The trade winds in the tropical North Atlantic enter the Caribbean Sea where the winds are intensified to form the Caribbean Low-Level Jet (CLLJ). Since pressure is low in the eastern North Pacific west of Central America and over North America, the easterly winds are thus split into two branches: One flowing westward across Central America and the other one flowing into the central United States via the western Gulf of Mexico (Figs. 2a and 2b). At the southern side of both the eastern Pacific and Atlantic ITCZ regions, as the air flow converges the southeasterly winds veer to the northeast becoming southwesterly in the far eastern Pacific and Atlantic south of 10°N (Figs. 2a and 2b). All of these features will be discussed in detail later.

The influence of the AWP on the NASH is demonstrated in Figs. 2c and 2d. The NASH is largely intensified after the AWP is removed (Fig. 2c). The SLP difference between the CTRL and NO_AWP runs shows negative values at the southwestern edge of the NASH extending westward to the southwest coast of the United States (Fig. 2d). This low pressure pattern results in westerly winds (the wind difference between the CTRL and NO_AWP runs) over the Caribbean and eastern North Pacific, and thus reduces the easterly CLLJ (see next section). Figure 2d also shows a northerly flow south of the Great Plains region (we will discuss this in detail in Section 5). The physical mechanism for the SLP's response to the AWP is explained in terms of Gill's (1980) simple theory. For an off-equatorial heating anomaly, Gill's theory predicts an atmospheric response involving low pressure to the northwest of the heating, associated with a Rossby wave. The AWP-induced SLP and wind in Fig. 2d are consistent with Gill's theoretical work [Wang and Lee (2007) test the consistency with Gill's dynamics]. In summary, our model results show that the role of the summertime AWP is to reduce the strength

of the NASH and thus also the CLLJ and CLLJ's branches into the eastern North Pacific and North America. As shown later, the weakening of SLP induced by the AWP is important for the distributions of low-level jets, moisture transport, rainfall, and tropospheric vertical wind shear in the tropical North Atlantic associated with tropical cyclones.

The time-longitude sections of SLP at 30°N are shown in Fig. 3. The seasonal SLP variations basically reflect seasonal heating/cooling over the continents and oceans. As the continents are heated (and the oceans are relatively cool) in the summer, a low-pressure system lies over continental North America, whereas the NASH is located in the eastern subtropical Atlantic Ocean. Both the NASH and the continental low intensify during the summer. In the winter, the NASH is weakened and extends westward to connect with the wintertime high pressure over continental North America. In additional to the winter westward extension, Figure 3a clearly shows a westward extension of the NASH in the midsummer and eastward migrations of the continental low in the spring and fall. These east-west excursions and the secondary NASH maximum in winter thus result in a semi-annual variation of the SLP in the regions of the Caribbean and Central America (Wang 2007), which in turn induces a change of the CLLJ (more on that later). Again, Figure 3c shows that the removal of the AWP strengthens the NASH and weakens the North American low. The seasonal dependence of the AWP's impact on SLP is clearly demonstrated in Fig. 3d. Two centers of negative SLP are located around 120°W and between 100°W-60°W. Maximum influence of the AWP on SLP occurs around September, reflecting that the size and intensity of the annual AWP are maximized in September (Wang and Enfield 2001, 2003; Fig. 1). Since most of Atlantic hurricanes occur during August to October (e.g., Gray 1984b), the maximum effect of the AWP on SLP implies that the AWP is an important factor for Atlantic hurricanes. We will revisit this issue in section 7.

4. Caribbean Low-Level Jet (CLLJ)

The NASH induces the easterly trade winds in the tropical North Atlantic. As the easterly trade winds enter into the western tropical North Atlantic, they can split into three branches into South, Central, and North Americas dependent on the season. During the winter, the easterly trade winds turn southward to supply moisture to rainfall associated with the South American monsoon (not shown since it is not a focus of this paper). Figure 4 shows the summer (JJA) vertically integrated moisture flux calculated from the NCEP-NCAR reanalysis and the CTRL ensemble run. The CAM3 model does a good job in simulating the pathways of the moisture flux transport, in comparison with the reanalysis field. During the summer, the easterly trade winds carry moisture from the tropical North Atlantic into the Caribbean Sea where the flow intensifies forming the easterly CLLJ (Fig. 4), due to a strong meridional pressure gradient set up by the NASH (Wang 2007). The CLLJ then splits into two branches: One turning northward and connecting with the Great Plains Low-Level Jet (GPLLJ), and the other one continuing westward across Central America into the eastern North Pacific. These two branches of moisture transport act to provide a linkage between the AWP and precipitation over the central United States and the eastern North Pacific, as will be shown later.

The detailed structure of the CLLJ can be further examined by plotting the vertical-meridional section of the zonal moisture transport distribution of qu (where q is specific humidity and u is zonal wind), as shown in Fig. 5. Comparison of Figs. 5a and 5b shows that the CAM3 model does a good job in simulating the zonal moisture transport. The CLLJ core of maximum westward moisture transport is located around 15°N at the lower troposphere (below 950 mb) extending to the surface. The CLLJ is, therefore, not only a conveyer belt for moisture,

but also a moisture collector that modulates surface evaporation and the moisture content it carries. As shown in Section 3, if the AWP is removed from the model-forcing SST, the NASH is strengthened. The strengthening of the NASH in turn intensifies the pressure gradient and then the CLLJ, which is indeed the case in our model ensemble run (Fig. 5c). The qu difference between the CTRL and NO_AWP runs in Fig. 5d shows a positive zonal moisture transport difference around the CLLJ region, indicating that the AWP is inversely related to the CLLJ's westward moisture transport. This supports the hypothesis that a large or warm (small or cold) AWP weakens (strengthens) the easterly CLLJ. This hypothesis is borne out by observations (Knaff 1997; Wang et al. 2006; Wang 2007).

The zonal moisture transport difference in Fig. 5d can be divided into three components contributed by (1) the zonal wind change $q\Delta u$, (2) the specific humidity change $u\Delta q$, and (3) the product of the zonal wind and specific humidity changes $\Delta u\Delta q$, where Δu (Δq) represents the zonal wind (specific humidity) difference between the CTRL and NO_AWP runs. Figure 6 shows the contribution of these three terms. The positive zonal moisture transport difference in Fig. 5d is mainly attributed to $q\Delta u$, whereas $u\Delta q$ makes a small contribution and $\Delta u\Delta q$ is negligible. That is, the AWP-induced zonal moisture transport around the CLLJ's core is largely due to the AWP-induced reduction of easterly wind.

The seasonal variations of the CLLJ's moisture transport at 75°W are shown in Fig. 7. Both the NCEP-NCAR reanalysis and the model show that the westward moisture transport between 10°N-20°N is maximized in the summer and winter, whereas it is minimized in the spring and fall (Figs. 7a and 7b). That is, the CLLJ's moisture transport has a semi-annual feature. Wang (2007) shows that the 925-mb zonal wind in the Caribbean region also displays a semi-annual variation. Early work on the CLLJ describes it as a single peak in the summer

(Amador 1998; Amador and Magana 1999). This paper, along with Wang (2007) and Wang and Lee (2007), is the first to document the semi-annual feature of the CLLJ and its westward moisture transport. As shown in Wang (2007) and Wang and Lee (2007), the semi-annual feature of the CLLJ follows the semi-annual cycle of SLP in the region of the Caribbean Sea that results from the east-west extension and development of the NASH. In other words, the high (low) pressure in the Caribbean during the summer and winter (spring and fall) results in the strong (weak) easterly CLLJ. The CLLJ is controlled by the meridional pressure gradient that is established by the NASH (Wang 2007).

The semi-annual feature of the zonal moisture transport in the Caribbean still exists for the model ensemble run with the AWP removed (Fig. 7c). The removal of the AWP only strengthens the amplitude of the CLLJ's westward moisture transport. These results are consistent with those of the atmospheric response to the AWP discussed earlier. As shown in Section 3, when the AWP is removed, the NASH is strengthened and the SLP in the Caribbean is increased (Fig. 2). However, the strengthening NASH still extends westward and eastward. In other words, the SLP in the Caribbean still has a semi-annual variation with the AWP removed. It is the east-west extension of the NASH that results in the semi-annual variation of SLP which in turn induces the semi-annual feature of the CLLJ's transport. Figure 7d shows the maximum AWP-induced reduction of the CLLJ's westward moisture transport occurring around September. Again, this is because the size and intensity of the annual AWP peak in the fall.

5. Great Plains Low-Level Jet (GPLLJ)

In the summer, atmospheric circulation of the northern mid-latitudes in the Western Hemisphere is dominated by the subtropical highs over ocean basins and the heated low pressure

over the continents. As can be seen from Fig. 2, the NASH and the North Pacific subtropical high reside in the eastern subtropical Atlantic and Pacific Oceans, respectively and low SLP is over continental North America. Associated with this SLP pattern are two northerly and two southerly low-level jets (Fig. 8a). Two northerly jets are located over eastern portion of the ocean basins, owing to the strong northerly winds at eastern edges of the subtropical highs. One of the southerly jets abuts the eastern slopes of the Sierra Madre Oriental range, which is called the Great Plains Low-Level Jet (GPLLJ). The other southerly jet is relatively weak and is centered along the southeast coast near 70°-80°W at the western edge of the NASH (hereafter referred to as the southeast jet).

The CAM3 model simulates these features reasonably well, as shown in Fig. 8b for the meridional wind at 30°N from the CTRL ensemble run. Impacts of the AWP on the GPLLJ and the southeast jet in the summer are displayed in Figs. 8c and 8d. A close inspection of Figs. 8b and 8c reveals that the southerly winds associated with the GPLLJ and the southeast jet are strengthened after the AWP is removed from the model forcing-SST. This is consistent with the pressure field of Fig. 2 in that the removal of the AWP strengthens SLP from the AWP region to the North American monsoon region. The feature of strengthening (or weakening with the AWP) southerly winds is clearly demonstrated by the meridional wind difference between the CTRL and NO_AWP runs in Fig. 8d, which shows a negative value of the wind difference around the GPLLJ. The model result is also consistent with that from the data analysis of Wang et al. (2006) who found a negative correlation between the anomalous AWP size and the 925-mb meridional wind anomalies in the central/eastern United States.

The two southerly jets transport moisture from the AWP to the central United States and to the United States southeastern seaboard where it becomes available for precipitation. Figure 9

shows the zonal-vertical sections of the meridional moisture transport distribution of qv at 30°N during the summer. Again, the CAM3 model does a reasonably good job in simulating the jet moisture transport (Figs. 9a and 9b). Figure 9d shows that the AWP tends to increase (decrease) the northward moisture transport above (below) the GPLLJ's core and to decrease the northward moisture transport of the southeast jet. What matters for precipitation is the vertically integrated moisture, so we examine the evolution of the vertically integrated meridional moisture transport at 30°N (Fig. 10). Figure 10 shows that the northward moisture transports associated with both the GPLLJ and the southeast jet are maximized in the summer when the continental North American low and the NASH reach their peaks (Fig. 3). After the summer, the northward moisture transports decay in response to their respective SLP variations. The prominent feature in Fig. 10d is that the AWP's effect is to increase the northward moisture transport associated with the GPLLJ in the summer and to decrease the transport in the fall.

Why does the AWP show an opposite effect on the meridional moisture transport in the summer and fall? This can be understood by dividing the meridional moisture transport difference into three components of: (1) the meridional wind change $q\Delta v$, (2) the specific humidity change $v\Delta q$, and (3) the product of the meridional wind and specific humidity changes $\Delta v\Delta q$, where Δv (Δq) represents the meridional wind (specific humidity) difference between the model CTRL and NO_AWP runs. Figures 11 and 12 show the contributions of these three terms during the summer and fall, respectively. For both the summer and fall, $\Delta v\Delta q$ is very small and negligible (Figs. 11c and 12c). The contribution of the meridional wind change $q\Delta v$ is negative near the GPLLJ during both the summer and fall (Figs. 11a and 12a), indicating that a reduction of the southerly wind reduces the northward moisture transport. However, the contribution of the specific humidity change $v\Delta q$ is positive during the summer (Fig. 11b),

whereas it is nearly zero in the fall (Fig. 12b). This reflects that the annual AWP's impact on the GPLLJ is always to weaken the southerly wind during the summer and fall. However, the impact on the specific humidity is to largely increase the specific humidity near the GPLLJ region in the summer and to be small (nearly zero) in the fall (not shown). The net result is an increase of specific humidity in the summer that overcomes the weakening of the southerly wind, and *vice versa* in the fall. Therefore, impact of the annual AWP is to increase the northward moisture transport to the central United States in the summer and to decrease the transport in the fall, as shown in Fig. 10d.

6. Rainfall

The precipitable water content in the atmosphere represents the amount of liquid water that would result if all the water vapor in the unit column of the atmosphere were condensed. Figure 13 shows the summer precipitable water distributions from the NCEP-NCAR reanalysis and our model runs. Since the capacity of the atmosphere to retain water vapor depends strongly on temperature, the precipitable water shows a general feature of a decrease with latitude similar to temperature distribution. As expected, the precipitable water is generally higher over the oceans than over the continents. The highest values of the precipitable water are over the eastern Pacific and Atlantic ITCZ regions, mainly due to strong ascending motion and high temperature there. Not surprisingly, the AWP region also shows a high value of the precipitable water during the summer when the annual warm pool is developed (Figs. 13a and 13b). Both the reanalysis and the model show that during the summer, a low amount of the precipitable water is over the west region of the United States. When the AWP is removed, our model run shows that the high value of the precipitable water over the AWP region disappears and that the precipitable water is

also reduced in the AWP's surrounding regions including the eastern Pacific ITCZ region (Figs. 13c and 13d). This indicates that the AWP contributes to a large amount of the precipitable water over the AWP and its surrounding regions.

The summertime rainfall pattern is roughly consistent with that of the precipitable water distribution in the atmosphere. Associated with the eastern Pacific and Atlantic ITCZs is heavy rainfall, as shown in Figs. 14a and 14b during the summer. Other summertime rainy features are over northern South America, Central America, the AWP region, the United States east of the Rocky Mountains, the United States Gulf Coast, and the United States southeastern seaboard. The west region of the United States, the western seaboard, and the subtropical high regions are mostly dry during the summer.

The summertime rainfall pattern can be explained in terms of the various atmospheric and oceanic features discussed above. The Atlantic and eastern Pacific ITCZs are associated with warm oceanic water, more precipitable water, and ascending atmospheric vertical motion, so heavy rainfall is observed there. The AWP and its surrounding regions (i.e., Central America, northern South America, and the United States Gulf Coast) are also expected to have more rainfall in the summer since the atmospheric precipitable water is high in these regions (Fig. 13). Both observations and the model results show that the northward moisture transport associated with the GPLLJ reaches maximum in the summer (Fig. 10). This maximum moisture transport is consistent with summertime rainfall observed over the Great Plains of the central United States (e.g., Mo and Berbery 2004; Mo et al. 2005).

The NASH and the North Pacific subtropical high during the summer are centered between 30°N-40°N and are strongest over the eastern portions of the ocean basins with isobars almost parallel to the east and west coasts of North America (Fig. 2). Thus, the subtropical highs

are associated with strong alongshore southerly (northerly) winds along the east (west) coast. Atmospheric Sverdrup balance [$\beta v = f\partial w / \partial z \approx -f(\partial u / \partial x + \partial v / \partial y)$] requires that planetary vorticity advection associated with southerly (northerly) winds is compensated by the vorticity tube stretching (shrinking) (e.g., Hoskins 1996; Seager et al. 2003). The east (west) coast is therefore associated with convergence (divergence) and ascending (subsiding) motions. These dynamically induced vertical motions can provide an explanation for the summertime wet (dry) rainfall pattern over the eastern (western) seaboard of North America shown in Figs. 14a and 14b [also see Nigam and Ruiz-Barradas (2006)].

The impacts of the AWP on summertime rainfall are shown in Figs. 14c and 14d. Figure 14d shows positive rainfall over the AWP region, the United States Gulf Coast region, and the east-central United States and negative rainfall west of Central America during the summer when the annual AWP is developed. An increase of rainfall in the United States east of the Rocky Mountains is consistent with indications that the AWP enhances the northward moisture transport of the GPLLJ during the summer (Fig. 10d). The negative rainfall in the far eastern Pacific west of Central America can be explained by the inverse relationship between the AWP and the CLLJ's westward moisture transport. As shown earlier, the CLLJ flows westward across Central America to supply moisture in the eastern Pacific and the AWP's effect is to reduce the CLLJ's westward moisture transport. The reduction of the westward moisture transport (the easterly wind) results in a moisture divergence (a reduction of evaporation) and thus the negative rainfall in the far eastern Pacific west of Central America (Fig. 14d).

The AWP's rainfall impacts can be discussed by the approximate balance of the atmospheric water vapor (Peixoto and Oort 1992): $P \approx E - \nabla \bullet \vec{Q}$, where P is precipitation, E is evaporation, and $\vec{Q} = \int_{300mb}^{sfc} (q\vec{u} / g)dp$ is the moisture flux vector (q is specific humidity, $\vec{u}$ is

vector wind, p is pressure, and g is gravity). The difference between the CTRL and NO_AWP runs are shown for the three terms in Fig. 15. In most regions, P is largely determined by the moisture convergence (Figs. 15a and 15b). However, E does contribute to rainfall, especially along the United States Gulf Coast, in the central United States and in the far eastern North Pacific (Figs. 15a and 15c).

As done previously, the moisture convergence difference in Fig. 15b is again divided into three contributions by: (1) the wind change, (2) the specific humidity change, and (3) the product of the wind and specific humidity changes (Fig. 16). A comparison of Fig. 16a and Fig. 15b shows that the moisture convergence pattern of Fig. 15b (and thus precipitation of Fig. 15a) is largely attributed to the wind change. This indicates that the effect of the AWP on the atmospheric circulation change is the most important for rainfall. The contribution of the specific humidity change to the moisture convergence shows a dipole pattern (Fig. 16b), with negative (positive) value in the AWP region (the eastern North Pacific). The moisture transport vector in Fig. 16 is also consistent with the moisture convergence distribution. Recall that the mean moisture transport in the Caribbean and eastern North Pacific is westward (Fig. 4). Figure 16 indicates that the AWP-induced specific humidity change strengthens the CLLJ's westward moisture transport, whereas the AWP-induced wind change weakens the transport. Therefore, the strengthening of the CLLJ's westward moisture transport by the specific humidity change decreases (increases) the moisture convergence to its upstream (downstream), and *vice versa* by the wind change.

7. Vertical wind shear associated with hurricanes

It is well accepted that a strong vertical wind shear between the upper and lower troposphere in the main development region (from 10°N to 20°N between the west coast of Africa to Central America) inhibits the formation and intensification of tropical cyclones (e.g., Gray 1968; Pasch and Avila 1992), probably as it relates to the organization of deep convection. Some studies argue that the vertical wind shear is remotely controlled by the equatorial eastern Pacific SST and Sahelian rainfall (e.g., Gray 1984a; Landsea and Gray 1992). Using observational data, Wang et al. (2006) show that the AWP is significantly correlated with the tropospheric vertical wind shear in the Atlantic hurricane main development region. When the AWP is large (small), the vertical wind shear is decreased (increased) and this is consistent with increased (decrease) Atlantic hurricane activity. The vertical wind shear distribution and the local AWP's influence on the vertical wind shear during August-October (ASO) are shown in Fig. 17. We focus on the months of ASO because most of Atlantic hurricanes that form in the main development region do so during ASO. In comparison with the mid-latitudes, the tropical and subtropical regions show a relatively low value of the vertical shear during ASO (Figs. 17a and 17b). If the AWP is removed, Figure 17c shows a large increase of the vertical wind shear in the subtropical region. The AWP's effect on the vertical wind shear is clearly seen in Fig. 17d that shows a longitudinal band of negative wind shear difference centered in the Caribbean. These model experiments suggest that the AWP is important for reducing the tropospheric vertical wind shear, thus favoring hurricane development and formation in ASO. This is consistent with the analysis of data by Wang et al. (2006).

How the AWP reduces the vertical wind shear is further demonstrated in Fig. 18. As discussed earlier, the atmospheric response to the AWP's heating is similar to Gill's dynamics

(Gill 1980). Figure 18 shows that the cyclonic circulation in the lower troposphere northwest of the AWP corresponds to an anticyclonic circulation in the upper troposphere. Thus, the AWP's effect is to reduce the easterly (westerly) winds of the lower (upper) troposphere in the Caribbean and the eastern North Pacific. The combination of the AWP-induced lower and upper tropospheric wind changes results in a large reduction of the vertical wind shear as shown in Fig. 17d.

8. Discussion and summary

The North Atlantic Subtropical High (NASH) and the North Pacific subtropical high are very important for determining atmospheric and oceanic circulations as well as the distribution of thermodynamical fields in the northern Western Hemisphere. In the summer, the subtropical highs are strong and centered in the eastern portions of the subtropical Atlantic and Pacific with a cell-type configuration. Sandwiched between the two highs over North America is a summertime continental low. The formation mechanisms of the subtropical highs are summarized in Miyasaka and Nakamura (2005; and references there) who emphasize that the summertime Pacific and Atlantic subtropical highs are mainly formed by the thermal contrast between the cool eastern ocean and the warm landmass to the east. Our model ensemble runs show that the AWP can influence the summertime SLP distribution in the Western Hemisphere. Consistent with Gill's (1980) theory, the atmospheric response to the AWP's heating is an atmospheric Rossby wave with low SLP centered to the northwest of the AWP. The AWP thus weakens the NASH with a largest decrease of SLP at its southwest edge, and it also strengthens the summertime continental low in the North American monsoon region. As part of the Gill response, a lower troposphere cyclone and upper troposphere anticyclone are vertically

juxtaposed over the Gulf of Mexico, leading to reduced vertical shear over their southern flank, i.e., the Caribbean.

Associated with the seasonal variation of the NASH is a semi-annual feature of SLP in the Caribbean region. Wang (2007) shows the seasonal east-west variation of the NASH. The NASH is strongest in the summer with a cell-type configuration extending toward the Caribbean. As the season progresses toward the fall, the NASH weakens and its center moves eastward. In the winter, since a continental high develops over North America, the NASH's isobars extend westward for connecting with the North American high. As the North American monsoon starts to develop in the spring, the NASH's isobars again retreat toward the east. This yearly movement and development of the NASH result in a semi-annual feature of SLP in the region of the Caribbean Sea.

The NASH produces the tropical easterly trade winds at its southern flank. When the easterly trade winds flow westward into the Caribbean Sea, the meridional pressure gradient set up by the NASH becomes large and thus the easterly winds intensify forming the easterly CLLJ (Wang 2007). Note that the land distribution is likely to be crucial to the intensification of the trade winds when they enter the Caribbean Sea. The possible effect of the land distribution on the CLLJ merits further study. Few studies are devoted to the CLLJ in the literature although it has the potential to affect weather and climate. Early papers on the CLLJ only mention and show its single peak in the summer (Amador 1998; Amador and Magana 1999). In this paper and Wang (2007) and Wang and Lee (2007), we find that the CLLJ and its westward moisture transport have a semi-annual feature: Two maxima in the summer and winter, and two minima in the spring and fall. This is because the SLP in the Caribbean region vary semi-annually in response to the east-west excursion of the NASH, as discussed above. That is, the high (low)

pressure in the Caribbean during the summer and winter (spring and fall) results in the strong (weak) easterly CLLJ and its westward moisture transport. The summertime CLLJ maximum is associated with the well-known mid-summer drought (MSD) in the region near Central America (Magana et al. 1999; Mapes et al. 2005) and a minimum of cyclogenesis in the Caribbean Sea (Inoue et al. 2002). This suggests that the high SLP and the strong easterly CLLJ in the Caribbean during the summer may be related to the MSD as well as the mid-season minimum of tropical cyclone activity reported previously.

The effect of the AWP on the CLLJ's moisture transport is to weaken it but not to change its semi-annual feature. This is consistent with our finding that the semi-annual feature of the CLLJ results from the twice yearly westward extension and eastward retreat of the NASH. The removal of the AWP does not terminate the zonal extension of the NASH, and it thus does not remove the semi-annual variation of the CLLJ and its transport. Both the NCEP-NCAR reanalysis and the model runs show that the easterly CLLJ continues to flow westward across Central America for supplying moisture in the eastern North Pacific. Our model results indeed show that the AWP-induced reduction of the CLLJ and its westward moisture transport is associated with a reduction of rainfall in the far eastern North Pacific west of Central America during the summer when the annual AWP is developed (Fig. 15a). However, when the annual AWP reaches its peak in the fall, the AWP-induced rainfall reduction pattern disappears and the entire eastern North Pacific is associated with positive rainfall response (not shown). This may suggest that the atmospheric response in the eastern North Pacific to the AWP depends on the phase of the AWP and the temporal variation of the eastern Pacific ITCZ.

In the AWP region the atmosphere has a high value of precipitable water during the summer because of its warm temperature. This is consistent with previous studies (e.g.

Rasmusson 1967; Brubaker et al 2001; and Mestas-Nuñez et al. 2005; Nigam and Ruiz-Barradas 2006) which suggest that the Intra-Americas Sea serves as a source of water vapor for rainfall in North, Central, and South Americas. High amounts of precipitable water can be exported to other places for rainfall if other atmospheric conditions are favorable. One of atmospheric phenomena responsible for northward summer moisture transport from the AWP into the United States east of the Rocky Mountains is the GPLLJ (Helfand and Schubert 1995; Mo et al. 1997; Ruiz-Barradas and Nigam 2005; Nigam and Ruiz-Barradas 2006). Many mechanisms have been hypothesized for the formation and maintenance of the GPLLJ [see a review by Stensrud (1996)]. One theory involves the orographic effect on the existence of the GPLLJ (Wexler 1961), which suggests that the GPLLJ's mechanism is similar to the western boundary currents in the ocean. This theory is supported by numerical model results (e.g., Byerle and Paegle 2003; Ting and Wang 2006). As the easterly trade winds reach the east slope of the Sierra Oriental, they turn northward. The vorticity conservation requires an increase in anticyclonic vorticity in order to compensate for the increase of planetary vorticity associated with a northward movement. Thus, an anticyclonic shear in the meridional northward flow develops, inducing a maximum northward jet.

Our model runs show that the AWP weakens the NASH and strengthens the continental low in the summer. Correspondingly, the southerly wind east of the Rocky Mountains (i.e., the GPLLJ) is weakened. However, the model runs show that the AWP impact is to enhance the northward moisture transport of the GPLLJ in the summer, owing to the fact that the meridional moisture transport is the product of the meridional wind and specific humidity. During the summer, the AWP induces a large increase of specific humidity east of the Rocky Mountains. The increase of specific humidity overcomes the weakening of the southerly GPLLJ, resulting in

an increase of the northward moisture transport during the summer when rainfall over the central United States reaches maximum (e.g., Mo and Berbery 2004).

In contrast to the summer, our model runs show that during the fall the AWP's impact is to weaken the GPLLJ's northward moisture transport. This is because the AWP induces a large weakening of the southerly wind east of the Rocky Mountains during the fall. However, the change in the specific humidity induced by the AWP is small in the fall. Therefore, the meridional moisture transport follows the meridional wind, showing a reduced effect of the AWP on the GPLLJ's northward moisture transport to the central United States during the fall.

Another low-level jet is found over the United States southeastern seaboard at the southwestern edge of the NASH. The strength of this southerly jet is controlled by the NASH. Since the NASH is strong in the summer, the southeast jet also peaks in the summer. The AWP's impact on this jet depends on the influence of the AWP on the NASH. Our model runs demonstrate that the AWP weakens the NASH and produces negative SLP at NASH's southwestern side which in turn decreases the southerly jet.

Since the water vapor transport occurs mainly in the lower troposphere, it is clearly affected by the earth's topography. Indeed, the existence of the Rocky Mountains parallel to the west coast of North America does not allow moisture from the Pacific Ocean to penetrate deeply into the American continent. Most of the summer moisture falling as precipitation east of the Rocky Mountains seem to be supplied by water vapor originating over the warm waters of the Gulf of Mexico, with a deep northward intrusion of water vapor (e.g., Helfand and Schubert 1995). Our model results demonstrate that this is indeed the case. When the AWP is removed from the model, rainfall over the central United States and the Gulf Coast region is reduced.

Consistent with the Gill's (1980) dynamics, the atmospheric response to the AWP's

heating is baroclinic. The AWP-induced cyclonic circulation in the lower troposphere is associated with the anticyclonic circulation in the upper troposphere. The AWP thus weakens the easterly trade winds in the tropical North Atlantic and the AWP also decreases the upper tropospheric westerly wind. This results in a decrease of the vertical wind shear between the upper and lower troposphere which favors hurricane development and formation during the hurricane season of ASO. Another issue that we would like to discuss is the influence of the AWP on the storm tracks. Since the AWP's effect is to decrease SLP at NASH's southwestern edge (i.e., the NASH shrinks toward the northeast), it is expected that a large AWP will allow more recurvature of Atlantic hurricanes. In other words, a large AWP does not allow the NASH to extend far west, meaning that hurricanes likely would be steered around NASH's edge to the north (instead of making landfall in the southeast United States). This issue needs to be studied further.

This paper focuses on the role of the annual AWP in the summer climate of the Western Hemisphere. A natural question to ask is what this may imply for interannual fluctuations of the AWP. We believe that most of the model results in this paper will be replicated correspondingly when they are model-tested on the interannual timescale. However, the moisture transport into the central United States via the GPLLJ merits further discussion. Mestas et al. (2006) show a negative correlation between northward moisture flux across the Gulf coast and SST anomalies in the Intra-Americas Sea during June-September, and a positive correlation between moisture flux and rainfall east of the Rockies Mountains, meaning reduced precipitation when the AWP is large. Their result is consistent with that of Wang et al. (2006) who show a negative correlation between the AWP size and rainfall anomalies over the central United States during ASO. The present paper shows that the annual AWP always weakens the southerly GPLLJ, consistent with

observations of Wang et al. (2006) and Mestas et al. (2006); however, the northward moisture transport of the GPLLJ is increased (decreased) during the summer (fall), suggesting that the offsetting influence of increased moisture over the Intra-Americas Sea is less important on the interannual time scale than for this model's representation of the annual AWP. The interannual relationship between the AWP and northward moisture transport needs to be studied further. We are currently investigating climate response to anomalously large and small AWPs and the result will be reported in a subsequent paper.

Acknowledgments. We thank three anonymous reviewers for their comments and suggestions that help improve the paper. This work was supported by a grant from National Oceanic and Atmospheric Administration (NOAA) Climate Program Office and by the base funding of NOAA Atlantic Oceanographic and Meteorological Laboratory (AOML). The findings and conclusions in this report are those of the author(s) and do not necessarily represent the views of the funding agency.

References

Amador, J. A., 1998: A climatic feature of the tropical Americas: The trade wind easterly jet. *Top. Meteor. Oceanogr.*, **5** (2), 1-13.

Amador, J. A., and V. Magana, 1999: Dynamics of the low level jet over the Caribbean Sea. Preprints, *The 23rd Conference on Hurricanes and Tropical Meteorology*, Dallas, TX, Amer. Meteor. Soc., 868-869.

Brubaker, K. L, P. A. Dirmeyer , A. Sudradjat, B. Levy and F. Bernal, 2001: A 36-yr climatological description of the evaporative sources of warm season precipitation in the Mississippi river basin. *J. Hydromet.*, **2**, 537-557.

Byerle, L. A., and J. Paegle, 2003: Modulation of the Great Plains low-level jet and moisture transports by orography and large-scale circulations. *J. Geophys. Res.*, **108** (D16), 8611, doi:10.1029/2002JD003005.

Collins, W. D., P. J. Rasch, B. A. Boville, J. J. Hack, J. R. McCaa, D. L. Williamson and B. P. Briegleb, 2006: The formulation and atmospheric simulation of the Community Atmospheric Model Version 3 (CAM3). *J. Climate*, **19**, 2144-2161.

Gill, A. E., 1980: Some simple solutions for heat-induced tropical circulation. *Quart. J. Roy. Meteor. Soc.*, **106**, 447-462.

Gray, W. M., 1968: Global view of the origions of tropical disturbances and storms. *Mon. Wea. Rev.*, **96**, 669-700.

Gray, W. M., 1984a: Atlantic seasonal hurricane frequency: Part I: El Niño and 30 mb quasi-biennial oscillation influences. *Mon. Wea. Rev.*, **112**, 1649-1668.

Gray W. M., 1984b: Atlantic seasonal hurricanes frequency. Part II: Forecasting its variability. *Mon. Wea. Rev.*, **112**, 1669-1683.

Helfand, H. M., and S. D. Schubert, 1995: Climatology of the simulated Great-Plains low level jet and its contribution to the continental moisture budget of the United-States. *J. Climate*, **8,** 784-806.

Hoskins, B. J., 1996: On the existence and strength of the summer subtropical anticyclones. *Bull. Amer. Meteor. Soc.*, **77**, 1287-1292.

Hurrell, J. W., J. J. Hack, A. S. Phillips, J. Caron, and J. Yin, 2006: The dynamical simulation of the Community Atmospheric Model Version 3 (CAM3). *J. Climate*, **19**, 2162-2183.

Inoue, M., I. C. Handoh, and G. R. Bigg, 2002: Bimodal distribution of tropical cyclogenesis in the Caribbean: Characteristics and environmental factors. *J. Climate*, **15**, 2897-2905.

Kalnay, E., and Co-authors, 1996: The NCEP/NCAR 40-year reanalysis project. *Bull. Am. Meteorol. Soc.*, **77**, 437-471.

Knaff, J. A., 1997: Implications of summertime sea level pressure anomalies in the tropical Atlantic region. *J. Climate*, **10**, 789-804.

Landsea, C. W., and W. M. Gray, 1992: The strong association between western Sahelian monsoon rainfall and intense Atlantic hurricanes. *J. Climate*, **5**, 435-453.

Magaña, V., J. A. Amador,, and S. Medina, 1999: The midsummer drought over Mexico and central America. *J. Climate,* **12**, 1577-1588.

Mapes, B. E., P. Liu, and N. Buenning, 2005: Indian monsoon onset and the Americas midsummer drought: Out-of-equilibrium response to smooth seasonal forcing. *J. Climate*, **18**, 1109-1115.

Miyasaka, T., and H. Nakamura, 2005: Structure and formation mechanisms of the Northern Hemisphere summertime subtropical highs. *J. Climate*, **18**, 5046-5065.

Mestas-Nunez, A. M., C. Zhang, and D. B. Enfield, 2005: Uncertainties in estimating moisture fluxes over the Intra-Americas Sea. *J. Hydrometeor.*, **6**, 696-709.

Mestas-Nunez, A. M., D. B. Enfield, and C. Zhang, 2006: Water vapor fluxes over the Intra-Americas Sea: Seasonal and interannual variability and associations with rainfall. *J. Climate*, accepted.

Mo, K. C., J. N. Paegle, and R. W. Higgins, 1997: Atmospheric processes associated with summer floods and droughts in the central United States. *J. Climate*, **10**, 3028-3046.

Mo, K. C., and E. H. Berbery, 2004: Low-level jets and the summer precipitation regimes over North America. *J. Geophys. Res.*, **109**, D06117, doi:10.1029/2003JD004106.

Mo, K. C., M. Chelliah, M. L. Carrera, R. W. Higgins, and W. Ebisuzaki, 2005: Atmospheric moisture transport over the United States and Mexico as evaluated in the NCEP regional reanalysis. *J. Hydrometeor.*, **6**, 710-728.

Nigam, S., and A. Ruiz-Barradas, 2006: Seasonal hydroclimate variability over North America in global and regional reanalysis and AMIP simulations: Varied representation. *J. Climate*, **19**, 815-837.

Pasch, R. J., and L. A. Avila, 1992: Atlantic hurricane season of 1991. *Mon. Wea. Rev.*, **120**, 2671-2687.

Peixoto, J. P., and A. H. Oort, 1992: *Physics of Climate*. American Institute of Physics, 520 pp.

Poveda, G., and O. J. Mesa, 1999: The low level westerly jet (Choco jet) and two other jets in Colombia: Climatology and variability during ENSO phases (in Spanish). Revista Academia Colombiana de Ciencias, **23 89**, 517–528.

Rasmusson, E. M., 1967: Atmospheric water vapor transport and the water balance of North America: Part I. Characteristics of the water vapor flux field. *Mon. Wea. Rev.*, **95,** 403-426.

Rayner, N. A., D. E. Parker, E. B. Horton, C. K. Folland, L. V. Alexander, D. P. Powell, E. C. Kent, and A. Kaplan, 2003: Global analysis of sea surface temperature, sea ice and night

marine air temperature since the late nineteenth century. *J. Geophys. Res.*, **108**, 4407, doi:10.1029/2002JD002670.

Ruiz-Barradas, A., and S. Nigam, 2005: Warm season rainfall variability over the US Great Plains in observations, NCEP and ERA-40 reanalysis, and NCAR and NASA atmospheric model simulations. *J. Climate*, **18**, 1808-1830.

Seager, R., R. Murtugudde, N. Naik, A. Clement, N. Gordon, and J. Miller, 2003: Air-sea interaction and seasonal cycle of the subtropical anticyclones. *J. Climate*, **16**, 1948-1966.

Stensrud, D. J., 1996: Importance of low-level jets to climate: A review. *J. Climate*, **9**, 1698-1711.

Ting, M., and H. Wang, 2006: The role of the North American topography on the maintenance of the Great Plains summer low-level jet. *J. Atmos. Sci.*, **63**, 1056-1068.

Wang, C., and D. B. Enfield, 2001: The tropical Western Hemisphere warm pool. *Geophys. Res. Lett.*, **28**, 1635-1638.

Wang, C., and D. B. Enfield, 2003: A further study of the tropical Western Hemisphere warm pool. *J. Climate,* **16**, 1476-1493.

Wang, C., D. B. Enfield, S.-K. Lee, and C. W. Landsea, 2006: Influences of the Atlantic warm pool on Western Hemisphere summer rainfall and Atlantic hurricanes. *J. Climate*, **19**, 3011-3028.

Wang, C., and S.-K. Lee, 2007: Atlantic warm pool, Caribbean low-level jet, and their potential impact on Atlantic hurricanes. *Geophys. Res. Lett.*, **34**, L02703, doi:10.1029/2006GL0028579.

Wang, C., 2007: Variability of the Caribbean low-level jet and its relations to climate. *Clim. Dyn.*, accepted.

Wexler, H., 1961: A boundary layer interpretation of the low-level jet. *Tellus*, **13**, 368-378.

Xie, P., and P.A. Arkin, 1997: Global precipitation: A 17-year monthly analysis based on gauge observations, satellite estimates, and numerical model outputs. *Bull. Am. Meteorol. Soc.*, **78**, 2539-2558.

Figure Captions

Figure 1. SST forcing difference between the CTRL and NO_AWP model runs in (a) March, (b) May, (c) July, and (d) September. The SST difference larger than 0.5°C is shaded. The AWP box (from 5°N to 30°N between 40°W and the coast of the Americas) is marked.

Figure 2. Horizontal structure of SLP (mb) and the 925-mb wind vector (m s^{-1}) during the summer of June-August (JJA) from (a) the NCEP-NCAR reanalysis, (b) the CTRL ensemble run, (c) the NO_AWP ensemble run, and (d) the difference between the CTRL and NO_AWP runs.

Figure 3. Time-longitude sections of SLP (mb) at 30°N from (a) the NCEP-NCAR reanalysis, (b) the CTRL ensemble run, (c) the NO_AWP ensemble run, and (d) the difference between the CTRL and NO_AWP runs. In (a)-(c), the SLP higher than 1018 mb is shaded and the contour interval is 2.0 mb. In (d), the negative SLP difference is shaded and the contour interval is 1.0 mb.

Figure 4. Summer (JJA) vertically integrated moisture flux ($\vec{Q} = \int_{300mb}^{sfc} (q\vec{u} / g)dp$, where q is specific humidity, $\vec{u}$ is vector wind, p is pressure, and g is gravity; in unit of kg m^{-1} s^{-1}) calculated from (a) the NCEP-NCAR reanalysis and (b) the CTRL ensemble run. Arrows indicate the moisture flux vector and colors represent the amplitude of the moisture flux.

Figure 5. Meridional-vertical sections of the zonal moisture transport of qu (g kg^{-1} m s^{-1}) at 75°W during the summer (JJA) from (a) the NCEP-NCAR reanalysis, (b) the CTRL ensemble run, (c) the NO_AWP ensemble run, and (d) the difference between the CTRL and NO_AWP runs. The unit on the vertical axis is mb. In (a)-(c), the westward moisture transport is shaded and the contour interval is 20 g kg^{-1} m s^{-1}. In (d), the positive moisture difference is shaded and the contour interval is 10 g kg^{-1} m s^{-1}.

Figure 6. Zonal moisture transport difference (g kg^{-1} m s^{-1}) between the CTRL and NO_AWP runs at 75°W during the summer (JJA) contributed by (a) the zonal wind change $q\Delta u$, (b) the specific humidity change $u\Delta q$, and (c) the product of the zonal wind and specific humidity changes $\Delta u\Delta q$. Δu (Δq) represents the zonal wind (specific humidity) difference between the CTRL and NO_AWP runs. The unit in the vertical direction is mb. The positive moisture difference is shaded and the contour interval is 10 g kg^{-1} m s^{-1}.

Figure 7. Time-latitude sections of the vertically integrated zonal moisture transport ($\int_{300\,mb}^{sfc}(qu/g)dp$; kg m^{-1} s^{-1}) at 75°W from (a) the NCEP-NCAR reanalysis, (b) the CTRL ensemble run, (c) the NO_AWP ensemble run, and (d) the difference between the CTRL and NO_AWP runs. In (a)-(c), the westward moisture transport is shaded and the contour interval is 50 kg m^{-1} s^{-1}. In (d), the positive moisture difference is shaded and the contour interval is 30 kg m^{-1} s^{-1}.

Figure 8. Zonal-vertical sections of the meridional wind of v (m s^{-1}) at 30°N during the summer (JJA) from (a) the NCEP-NCAR reanalysis, (b) the CTRL ensemble run, (c) the NO_AWP

ensemble run, and (d) the difference between the CTRL and NO_AWP runs. The unit on the vertical axis is mb. In (a)-(c), the northward wind is shaded and the contour interval is 1.0 m s^{-1}. In (d), the positive wind difference is shaded and the contour interval is 0.3 m s^{-1}.

Figure 9. Zonal-vertical sections of the meridional moisture transport of qv (g kg^{-1} m s^{-1}) at 30°N during the summer (JJA) from (a) the NCEP-NCAR reanalysis, (b) the CTRL ensemble run, (c) the NO_AWP ensemble run, and (d) the difference between the CTRL and NO_AWP runs. The unit on the vertical axis is mb. In (a)-(c), the northward moisture transport is shaded and the contour interval is 10 g kg^{-1} m s^{-1}. In (d), the positive moisture transport difference is shaded and the contour interval is 3 g kg^{-1} m s^{-1}.

Figure 10. Time-longitude sections of the vertically integrated meridional moisture transport ($\int_{300\,mb}^{sfc}(qv/g)dp$; kg m^{-1} s^{-1}) at 30°N from (a) the NCEP-NCAR reanalysis, (b) the CTRL ensemble run, (c) the NO_AWP ensemble run, and (d) the difference between the CTRL and NO_AWP runs. In (a)-(c), the northward moisture transport is shaded and the contour interval is 20 kg m^{-1} s^{-1}. In (d), the positive moisture transport is shaded and the contour interval is 10 kg m^{-1} s^{-1}.

Figure 11. Meridional moisture transport difference (g kg^{-1} m s^{-1}) between the CTRL and NO_AWP runs at 30°N during June-August (JJA) contributed by (a) the meridional wind change $q\Delta v$, (b) the specific humidity change $v\Delta q$, and (c) the product of the meridional wind and specific humidity changes $\Delta v\Delta q$. Δv (Δq) represents the meridional wind (specific humidity)

difference between the CTRL and NO_AWP runs. The unit on the vertical axis is mb. The positive moisture transport difference is shaded and the contour interval is 3 g kg^{-1} m s^{-1}.

Figure 12. Meridional moisture transport difference (g kg^{-1} m s^{-1}) between the CTRL and NO_AWP runs at 30°N during September-October (SO) contributed by (a) the meridional wind change $q\Delta v$, (b) the specific humidity change $v\Delta q$, and (c) the product of the meridional wind and specific humidity changes $\Delta v\Delta q$. Δv (Δq) represents the meridional wind (specific humidity) difference between the CTRL and NO_AWP runs. The unit on the vertical axis is mb. The positive moisture transport difference is shaded and the contour interval is 3 g kg^{-1} m s^{-1}.

Figure 13. Summer (JJA) precipitable water content (kg m^{-2}) from (a) the NCEP-NCAR reanalysis, (b) the CTRL ensemble run, (c) the NO_AWP ensemble run, and (d) the difference between the CTRL and NO_AWP runs. In (a)-(c), the precipitable water content larger than 30 kg m^{-2} is shaded and the contour interval is 5 kg m^{-2}. In (d), the positive precipitable water difference is shaded and the contour interval is 2.5 kg m^{-2}.

Figure 14. Summer (JJA) rainfall (mm day^{-1}) distribution from (a) the CMAP product, (b) the CTRL ensemble run, (c) the NO_AWP ensemble run, and (d) the difference between the CTRL and NO_AWP runs. In (a)-(c), the rainfall larger than 2.0 mm day^{-1} is shaded and the contour interval is 2 mm day^{-1}. In (d), the positive rainfall difference is shaded and the contour interval is 1.0 mm day^{-1}.

Figure 15. Precipitation, moisture convergence [$-\nabla\bullet\vec{Q}$, where $\vec{Q}=\int_{300mb}^{sfc}(q\vec{u}/g)dp$], and evaporation. Shown is the difference between the CTRL and NO_AWP runs for (a) precipitation (mm day^{-1}), (b) moisture convergence (mm day^{-1}), and (c) evaporation (mm day^{-1}). The positive value is shaded and the contour interval is 1.0 mm day^{-1}.

Figure 16. The moisture convergence (contour; mm day^{-1}) and transport (vector; kg m^{-1} s^{-1}) difference between the CTRL and NO_AWP runs during June-August (JJA) contributed by (a) the wind change $\left(-\nabla\bullet\left[\int_{300mb}^{sfc}(q\Delta\vec{u}/g)dp\right]\right.$ and $\left.\int_{300mb}^{sfc}(q\Delta\vec{u}/g)dp\right)$, (b) the specific humidity change $\left(-\nabla\bullet\left[\int_{300mb}^{sfc}(\vec{u}\Delta q/g)dp\right]\right.$ and $\left.\int_{300mb}^{sfc}(\vec{u}\Delta q/g)dp\right)$, and (c) the product of the wind and specific humidity changes $\left(-\nabla\bullet\left[\int_{300mb}^{sfc}(\Delta q\Delta\vec{u}/g)dp\right]\right.$ and $\left.\int_{300mb}^{sfc}(\Delta q\Delta\vec{u}/g)dp\right)$. $\Delta\vec{u}$ (Δq) represents the wind vector (specific humidity) difference between the CTRL and NO_AWP runs.

Figure 17. Tropospheric vertical wind shear ($\left[(U_{200}-U_{850})^2+(V_{200}-V_{850})^2\right]^{1/2}$; m s^{-1}) during August-October (ASO) from (a) the NCEP-NCAR reanalysis, (b) the CTRL ensemble run, (c) the NO_AWP ensemble run, and (d) the difference between the CTRL and NO_AWP runs.

Figure 18. Geopotential height (10^2 m) and wind (m s^{-1}) difference between the CTRL and NO_AWP runs during August-October (ASO) at (a) 200-mb and (b) 850-mb.

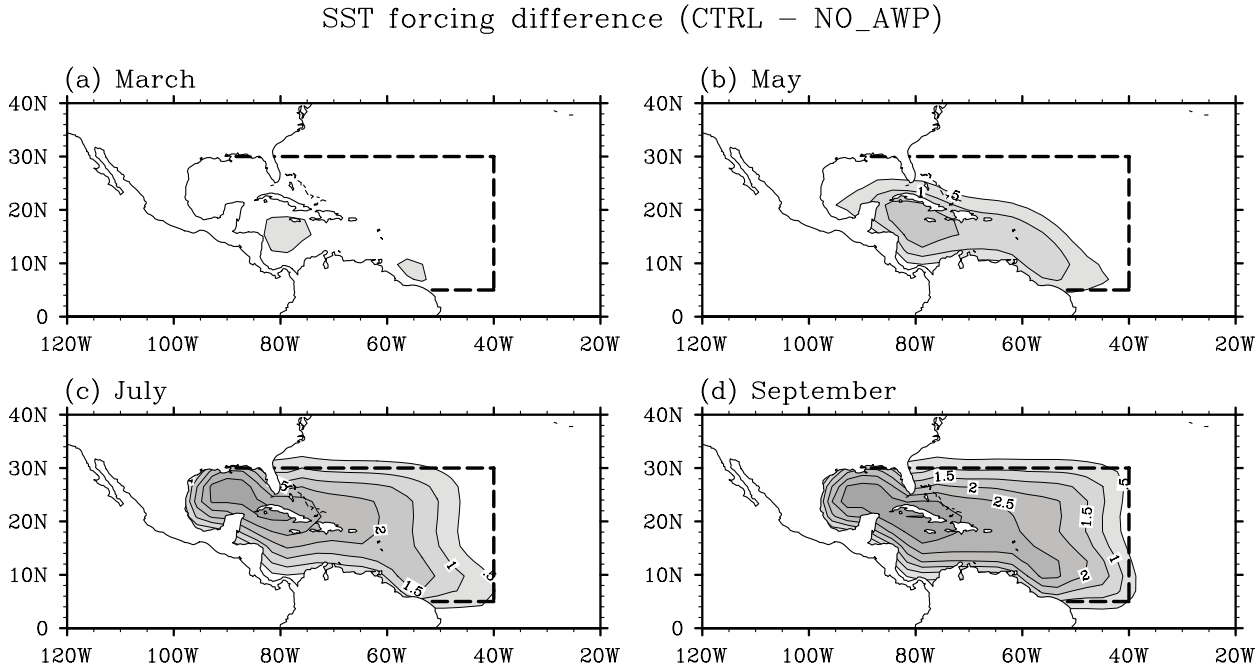

Figure 1. SST forcing difference between the CTRL and NO_AWP model runs in (a) March, (b) May, (c) July, and (d) September. The SST difference larger than 0.5°C is shaded. The AWP box (from 5°N to 30°N between 40°W and the coast of the Americas) is marked.

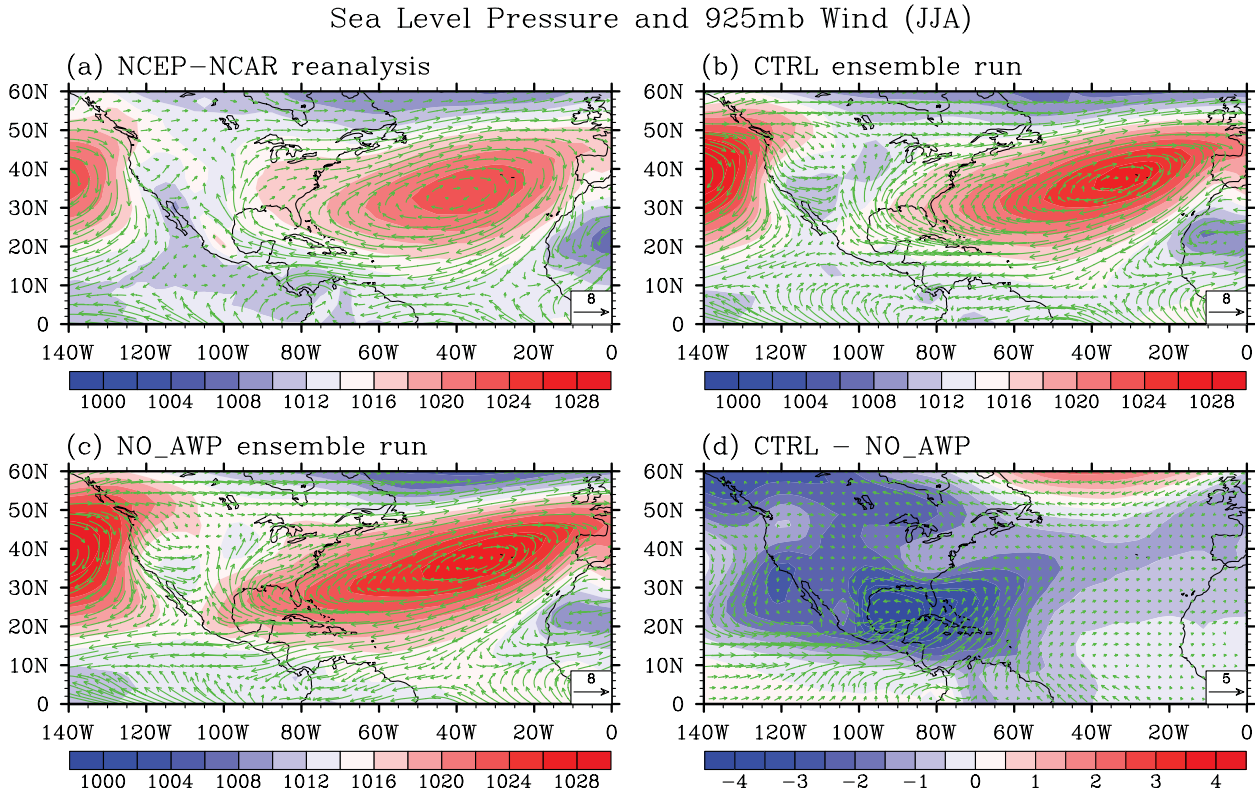

Figure 2. Horizontal structure of SLP (mb) and the 925-mb wind vector (m s^{-1}) during the summer of June-August (JJA) from (a) the NCEP-NCAR reanalysis, (b) the CTRL ensemble run, (c) the NO_AWP ensemble run, and (d) the difference between the CTRL and NO_AWP runs.

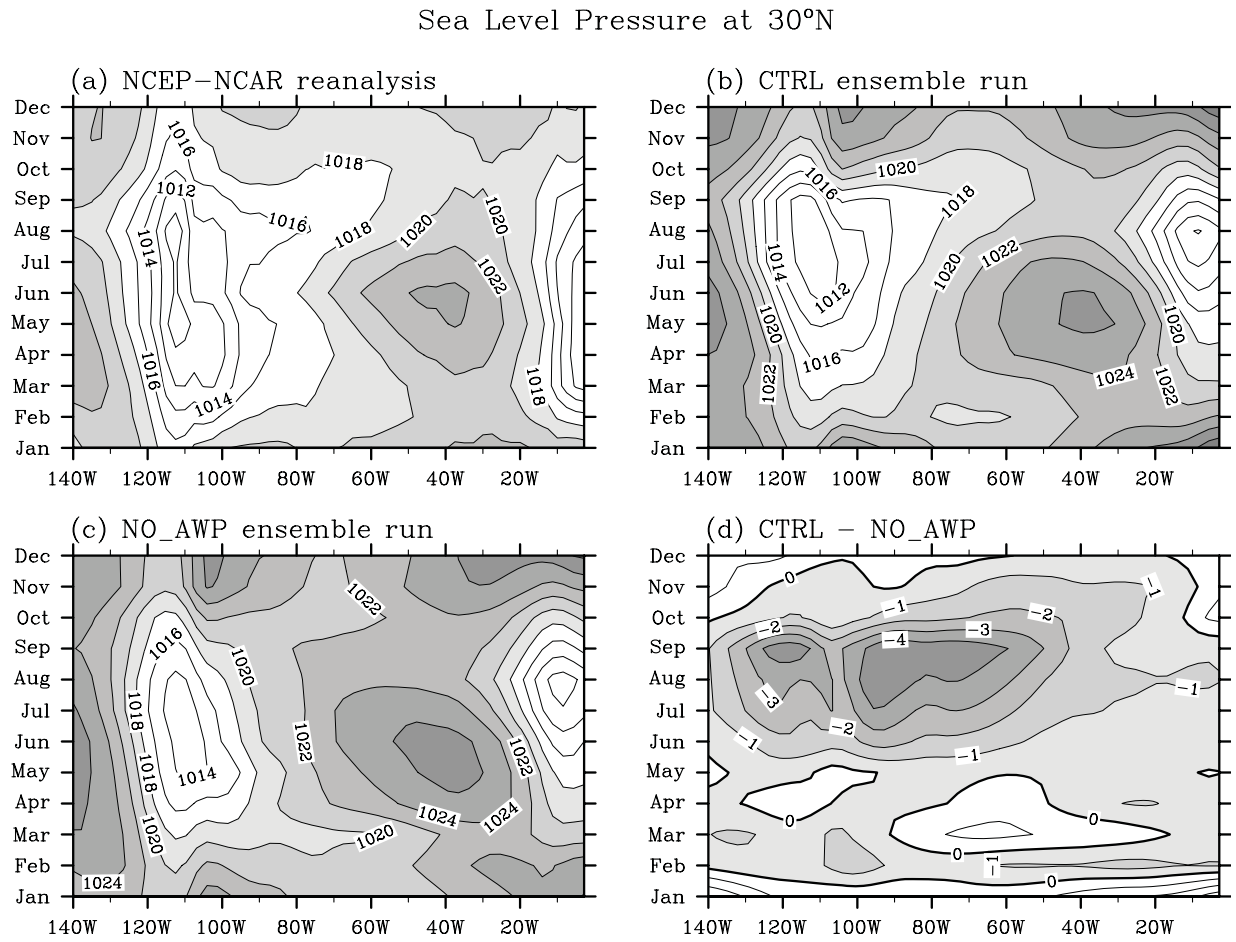

Figure 3. Time-longitude sections of SLP (mb) at 30°N from (a) the NCEP-NCAR reanalysis, (b) the CTRL ensemble run, (c) the NO_AWP ensemble run, and (d) the difference between the CTRL and NO_AWP runs. In (a)-(c), the SLP higher than 1018 mb is shaded and the contour interval is 2.0 mb. In (d), the negative SLP difference is shaded and the contour interval is 1.0 mb.

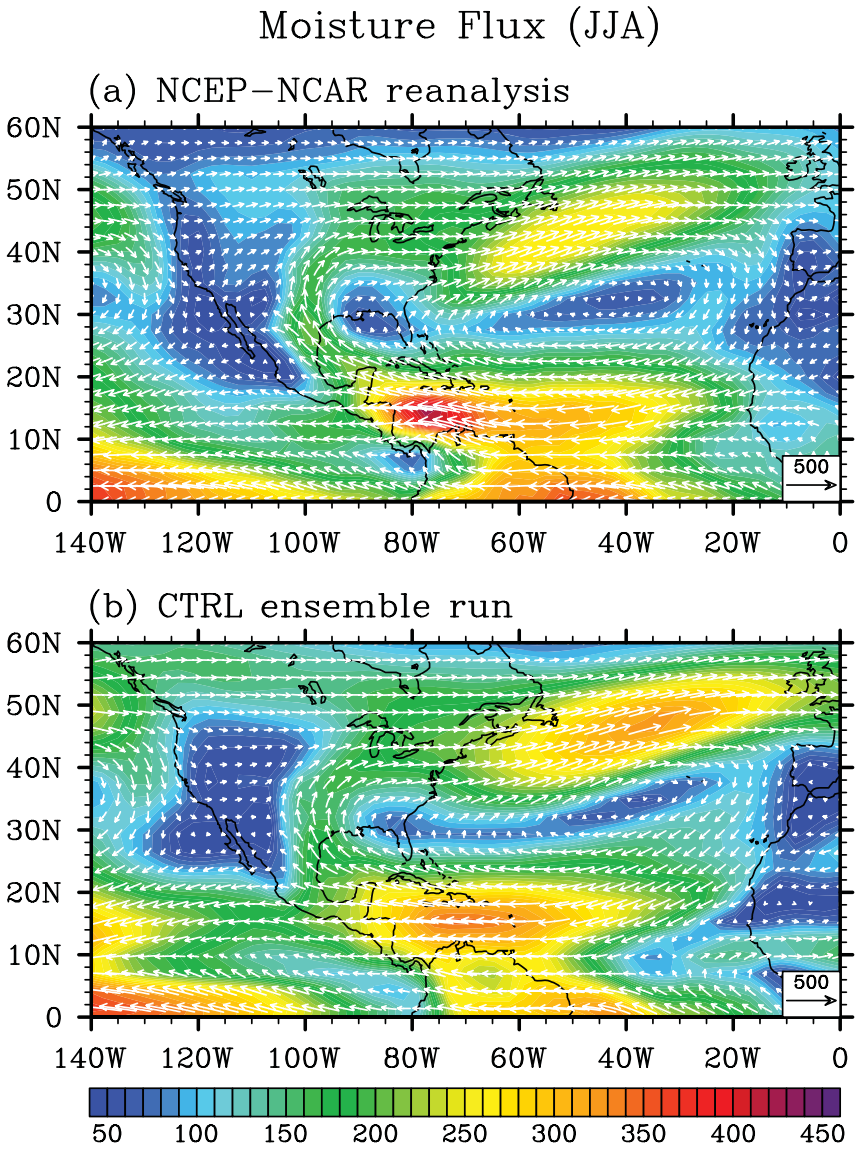

Figure 4. Summer (JJA) vertically integrated moisture flux ($\vec{Q} = \int_{300mb}^{sfc} (q\vec{u} / g)dp$, where q is specific humidity, $\vec{u}$ is vector wind, p is pressure, and g is gravity; in unit of kg m^{-1} s^{-1}) calculated from (a) the NCEP-NCAR reanalysis and (b) the CTRL ensemble run. Arrows indicate the moisture flux vector and colors represent the amplitude of the moisture flux.

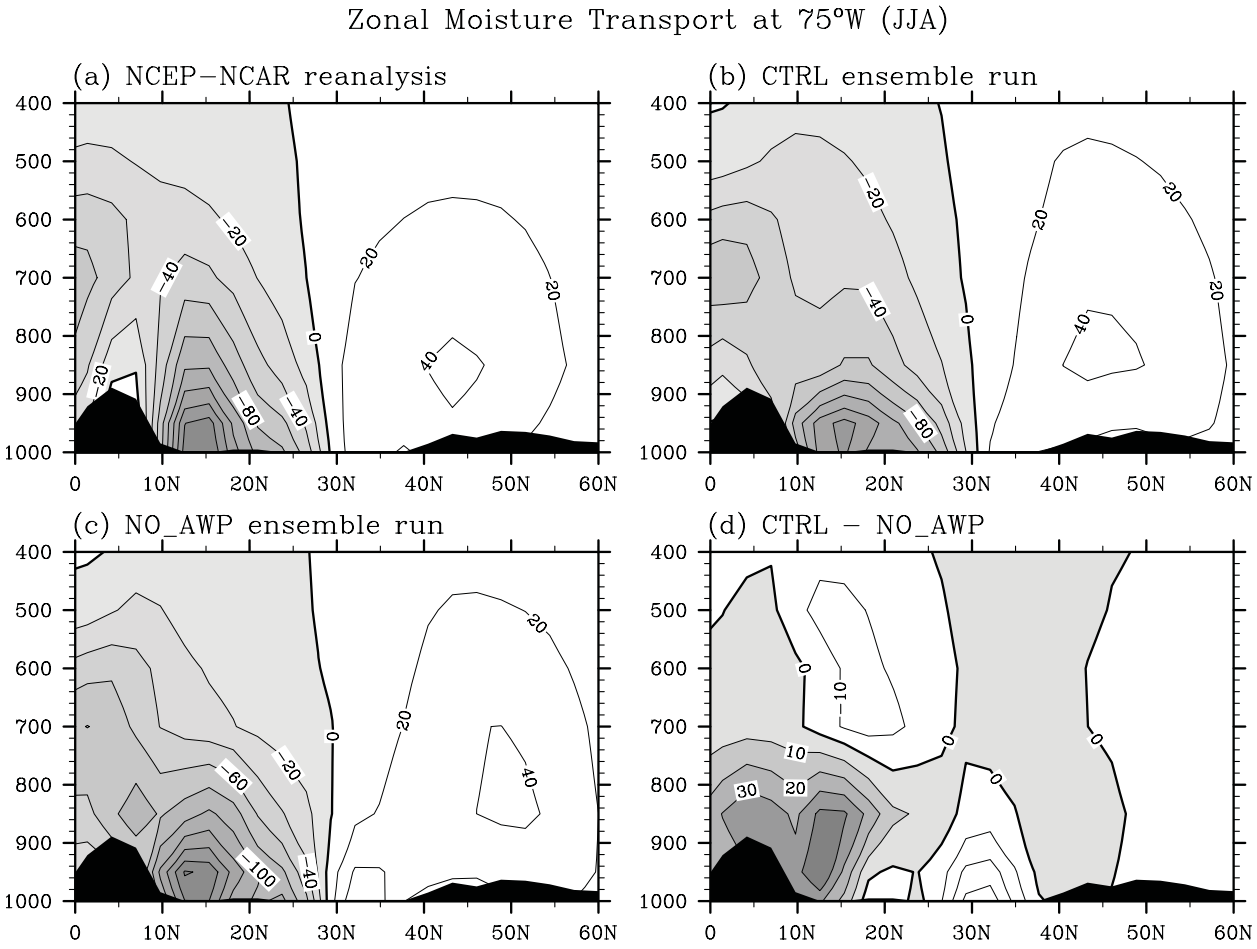

Figure 5. Meridional-vertical sections of the zonal moisture transport of *qu* (g kg^{-1} m s^{-1}) at 75°W during the summer (JJA) from (a) the NCEP-NCAR reanalysis, (b) the CTRL ensemble run, (c) the NO_AWP ensemble run, and (d) the difference between the CTRL and NO_AWP runs. The unit on the vertical axis is mb. In (a)-(c), the westward moisture transport is shaded and the contour interval is 20 g kg^{-1} m s^{-1}. In (d), the positive moisture difference is shaded and the contour interval is 10 g kg^{-1} m s^{-1}.

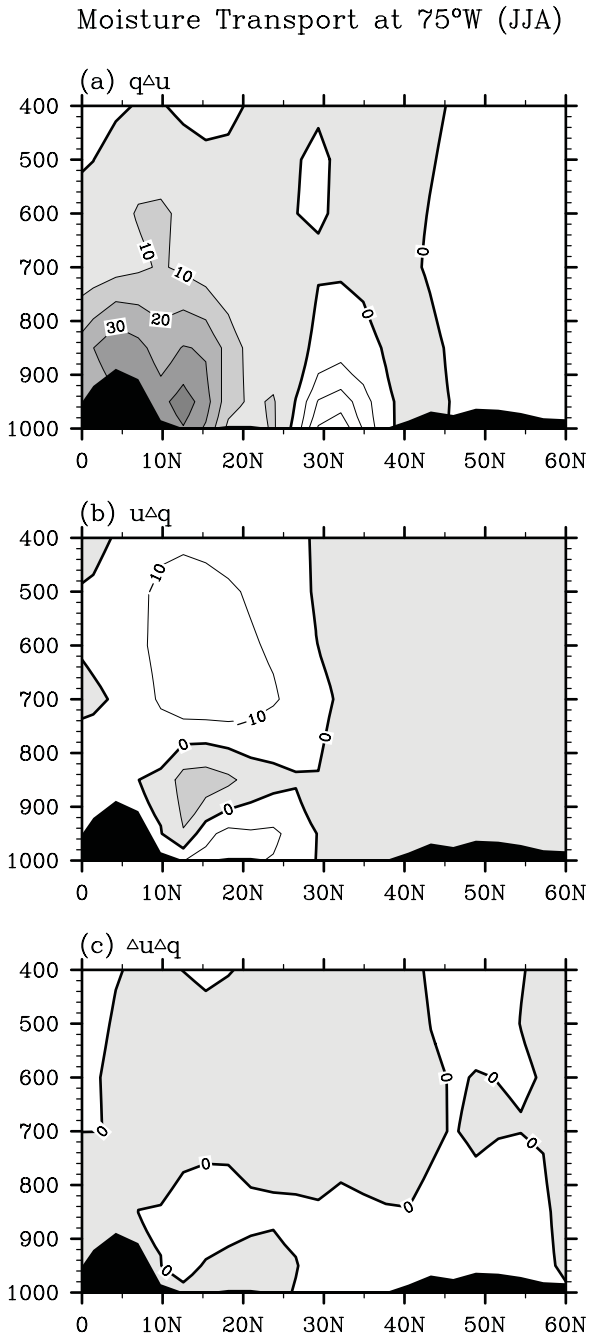

Figure 6. Zonal moisture transport difference (g kg^{-1} m s^{-1}) between the CTRL and NO_AWP runs at 75°W during the summer (JJA) contributed by (a) the zonal wind change $q\Delta u$, (b) the specific humidity change $u\Delta q$, and (c) the product of the zonal wind and specific humidity changes $\Delta u\Delta q$. Δu (Δq) represents the zonal wind (specific humidity) difference between the CTRL and NO_AWP runs. The unit in the vertical direction is mb. The positive moisture difference is shaded and the contour interval is 10 g kg^{-1} m s^{-1}.

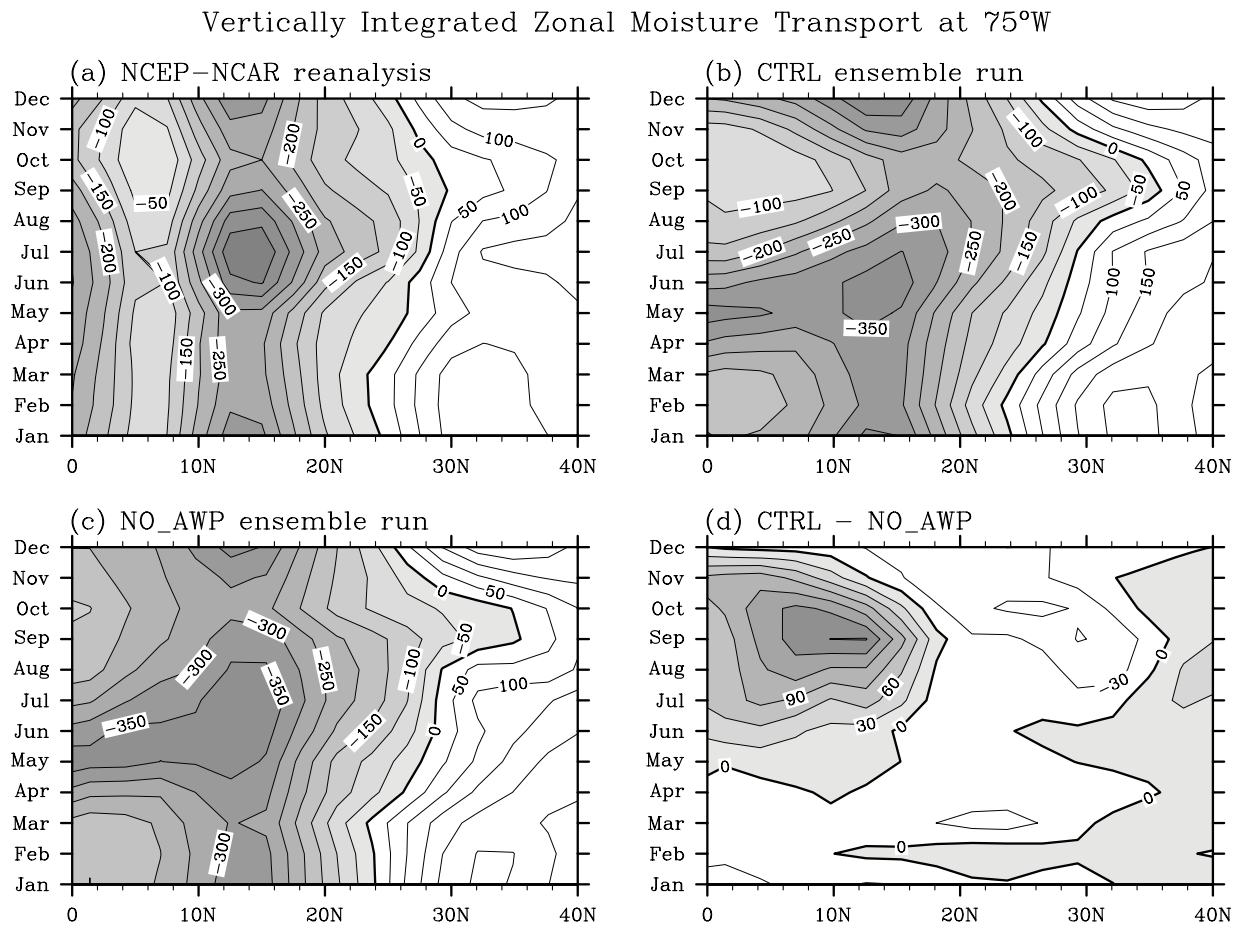

Figure 7. Time-latitude sections of the vertically integrated zonal moisture transport ($\int_{300mb}^{sfc}(qu/g)dp$; kg m^{-1} s^{-1}) at 75°W from (a) the NCEP-NCAR reanalysis, (b) the CTRL ensemble run, (c) the NO_AWP ensemble run, and (d) the difference between the CTRL and NO_AWP runs. In (a)-(c), the westward moisture transport is shaded and the contour interval is 50 kg m^{-1} s^{-1}. In (d), the positive moisture difference is shaded and the contour interval is 30 kg m^{-1} s^{-1}.

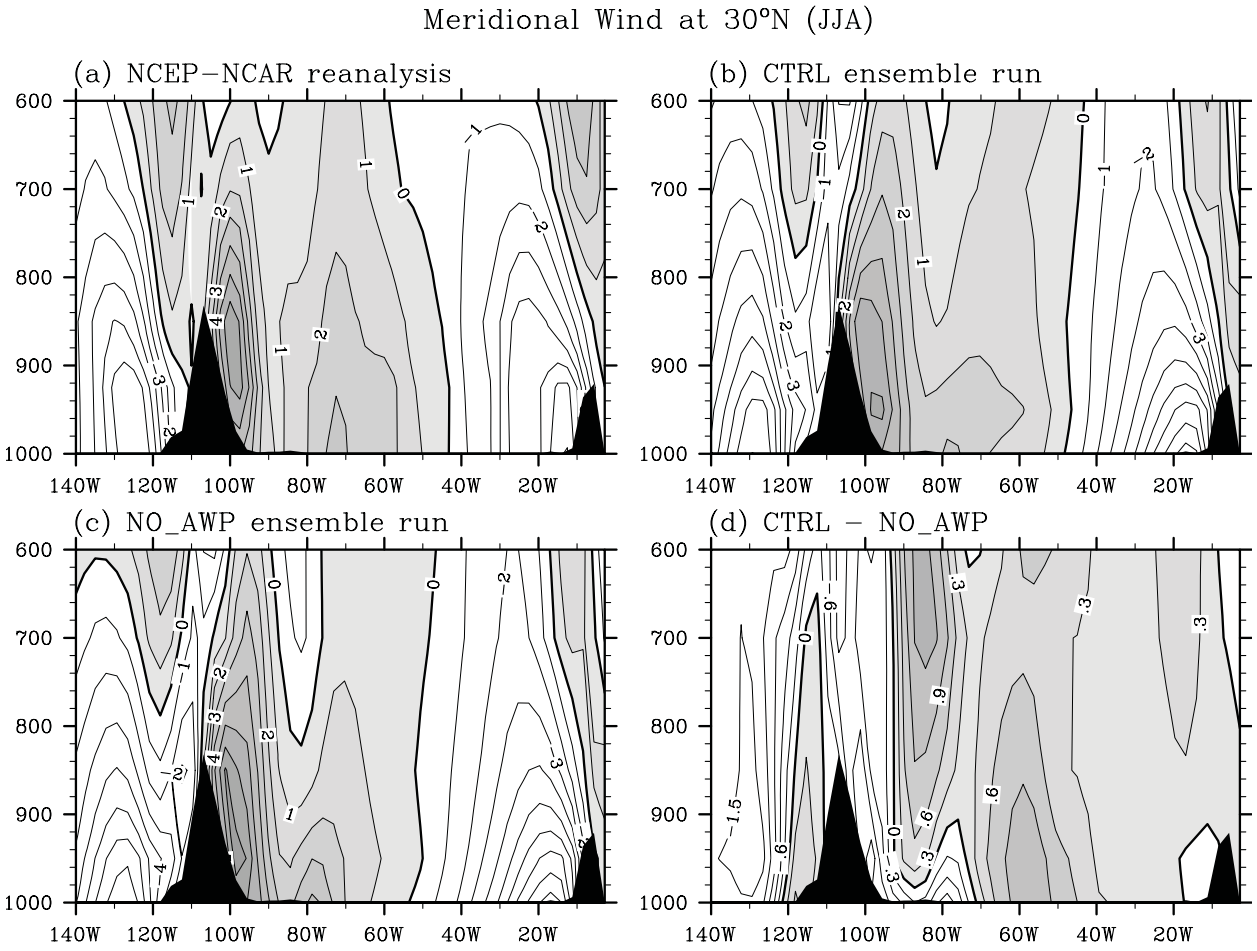

Figure 8. Zonal-vertical sections of the meridional wind of v (m s^{-1}) at 30°N during the summer (JJA) from (a) the NCEP-NCAR reanalysis, (b) the CTRL ensemble run, (c) the NO_AWP ensemble run, and (d) the difference between the CTRL and NO_AWP runs. The unit on the vertical axis is mb. In (a)-(c), the northward wind is shaded and the contour interval is 1.0 m s^{-1}. In (d), the positive wind difference is shaded and the contour interval is 0.3 m s^{-1}.

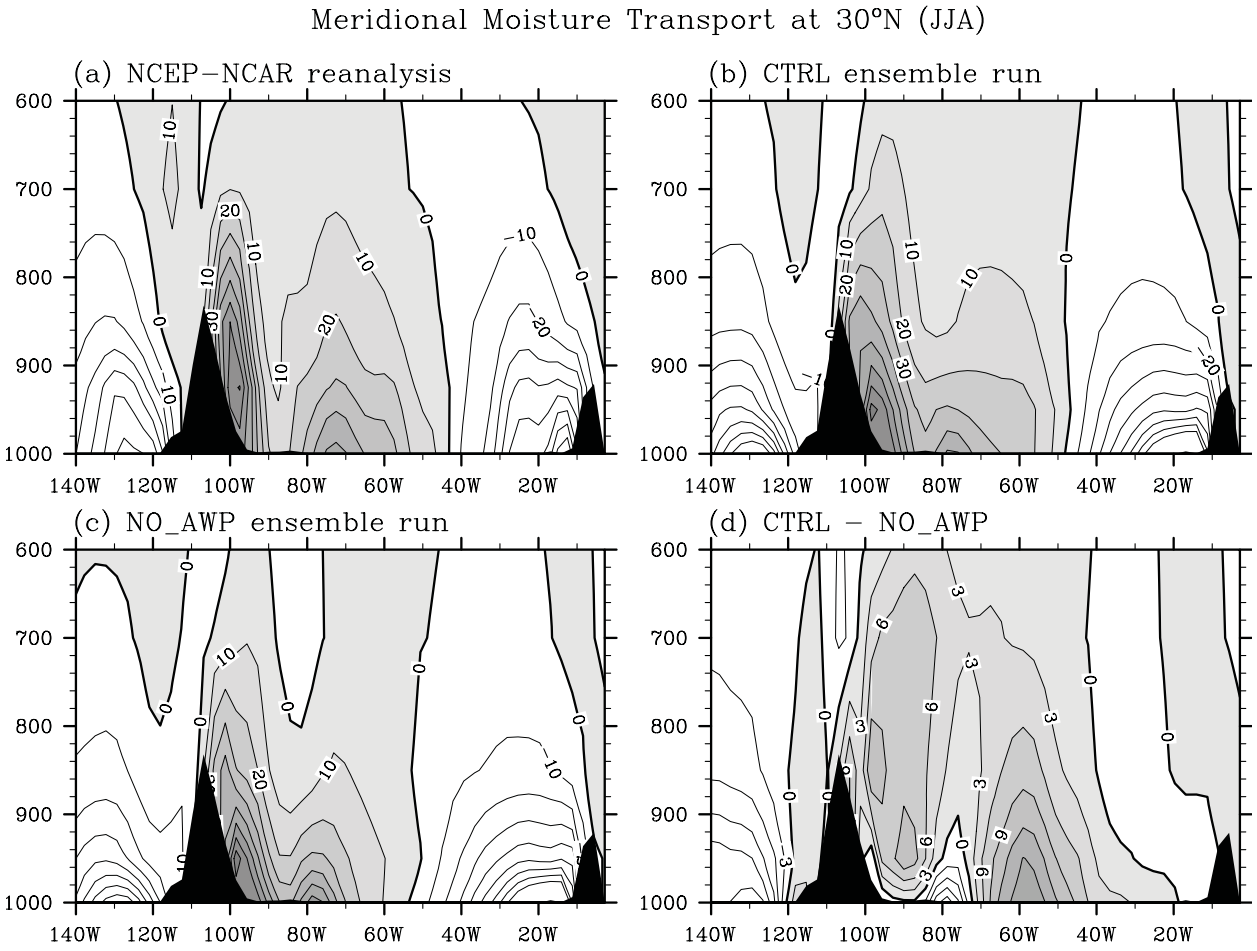

Figure 9. Zonal-vertical sections of the meridional moisture transport of qv (g kg^{-1} m s^{-1}) at 30°N during the summer (JJA) from (a) the NCEP-NCAR reanalysis, (b) the CTRL ensemble run, (c) the NO_AWP ensemble run, and (d) the difference between the CTRL and NO_AWP runs. The unit on the vertical axis is mb. In (a)-(c), the northward moisture transport is shaded and the contour interval is 10 g kg^{-1} m s^{-1}. In (d), the positive moisture transport difference is shaded and the contour interval is 3 g kg^{-1} m s^{-1}.

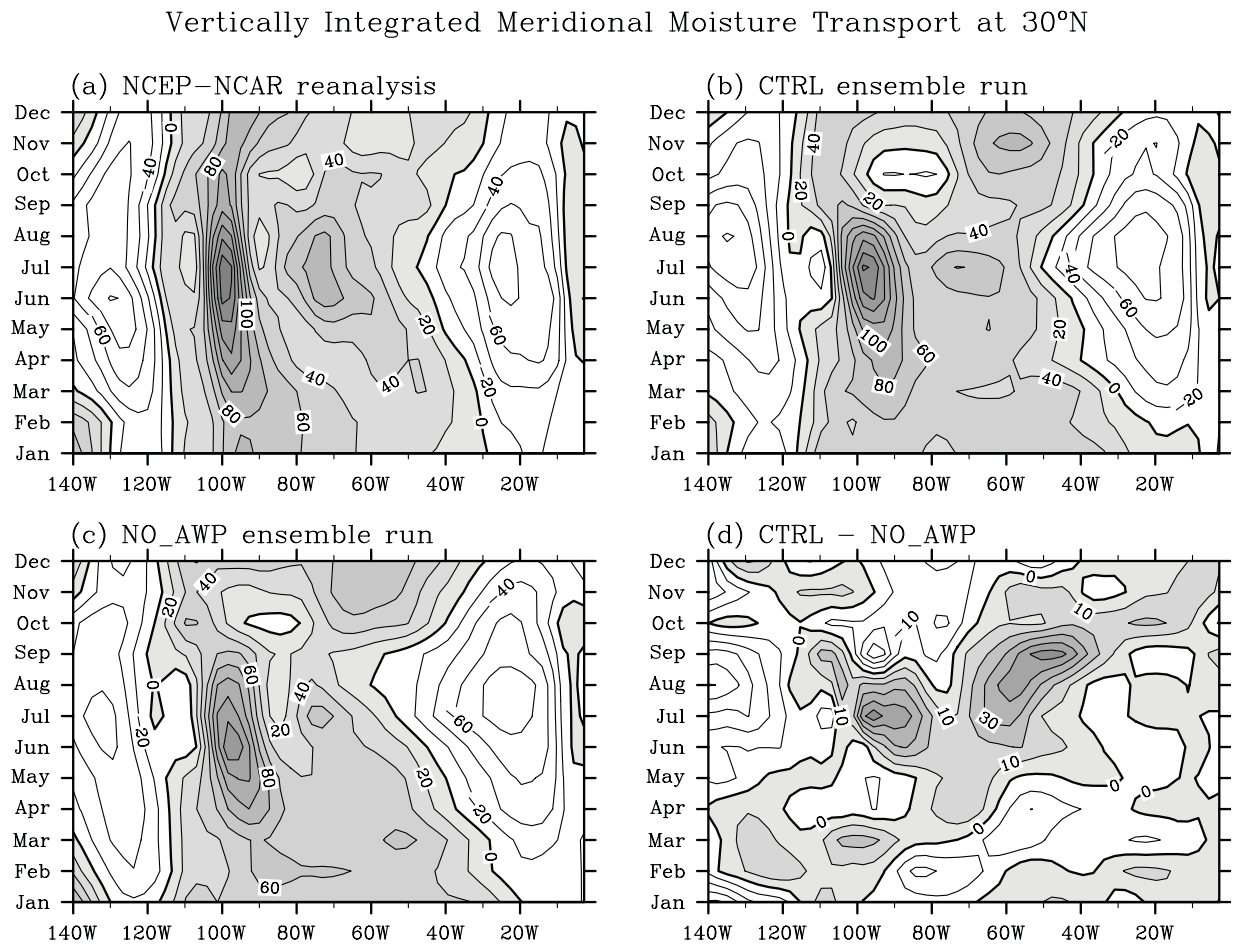

Figure 10. Time-longitude sections of the vertically integrated meridional moisture transport ($\int_{300\,mb}^{sfc}(qv/g)dp$; kg m^{-1} s^{-1}) at 30°N from (a) the NCEP-NCAR reanalysis, (b) the CTRL ensemble run, (c) the NO_AWP ensemble run, and (d) the difference between the CTRL and NO_AWP runs. In (a)-(c), the northward moisture transport is shaded and the contour interval is 20 kg m^{-1} s^{-1}. In (d), the positive moisture transport is shaded and the contour interval is 10 kg m^{-1} s^{-1}.

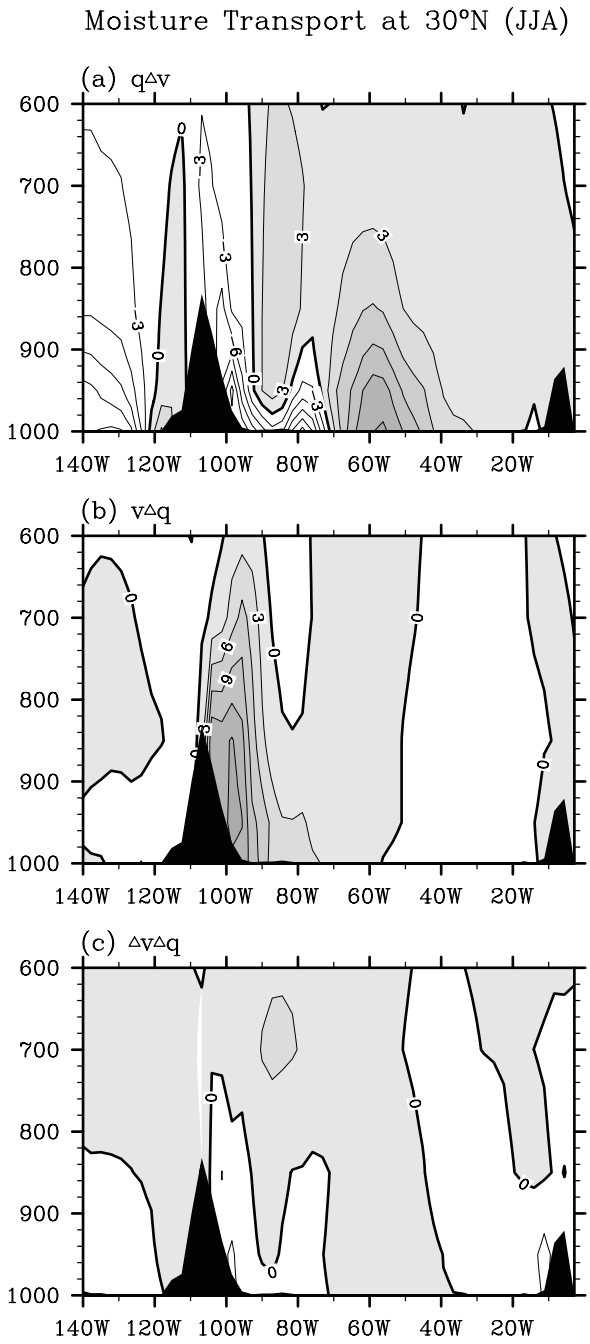

Figure 11. Meridional moisture transport difference (g kg^{-1} m s^{-1}) between the CTRL and NO_AWP runs at 30°N during June-August (JJA) contributed by (a) the meridional wind change $q\Delta v$, (b) the specific humidity change $v\Delta q$, and (c) the product of the meridional wind and specific humidity changes $\Delta v\Delta q$. Δv (Δq) represents the meridional wind (specific humidity) difference between the CTRL and NO_AWP runs. The unit on the vertical axis is mb. The positive moisture transport difference is shaded and the contour interval is 3 g kg^{-1} m s^{-1}.

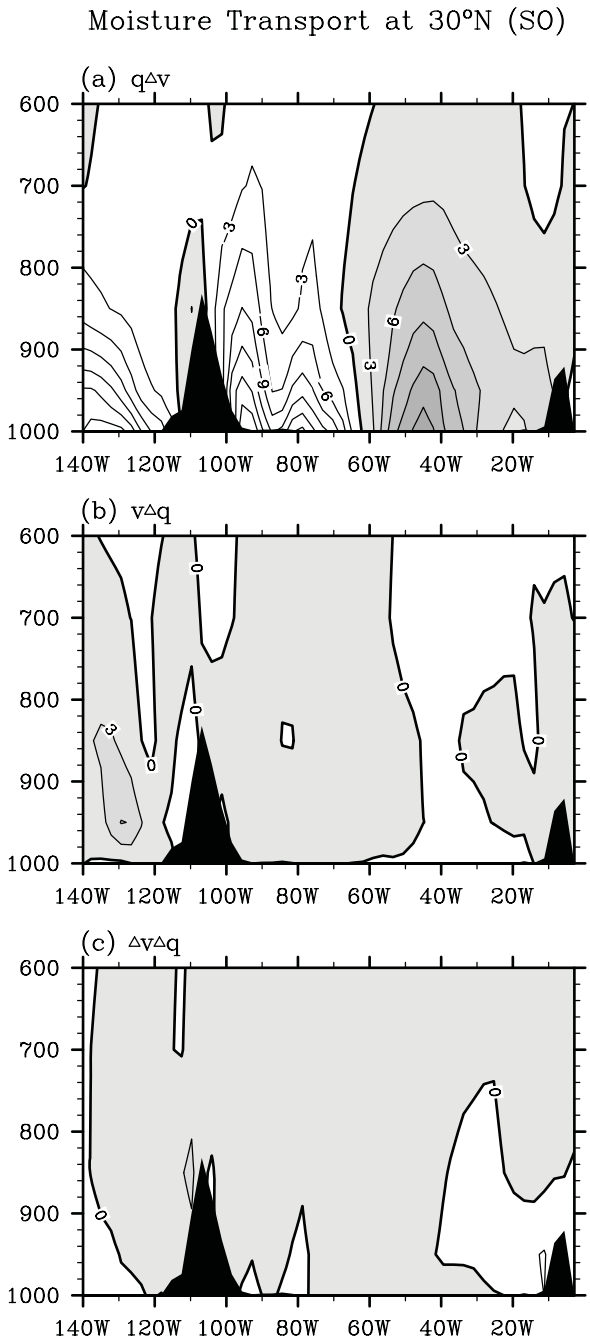

Figure 12. Meridional moisture transport difference (g kg^{-1} m s^{-1}) between the CTRL and NO_AWP runs at 30°N during September-October (SO) contributed by (a) the meridional wind change $q\Delta v$, (b) the specific humidity change $v\Delta q$, and (c) the product of the meridional wind and specific humidity changes $\Delta v\Delta q$. Δv (Δq) represents the meridional wind (specific humidity) difference between the CTRL and NO_AWP runs. The unit on the vertical axis is mb. The positive moisture transport difference is shaded and the contour interval is 3 g kg^{-1} m s^{-1}.

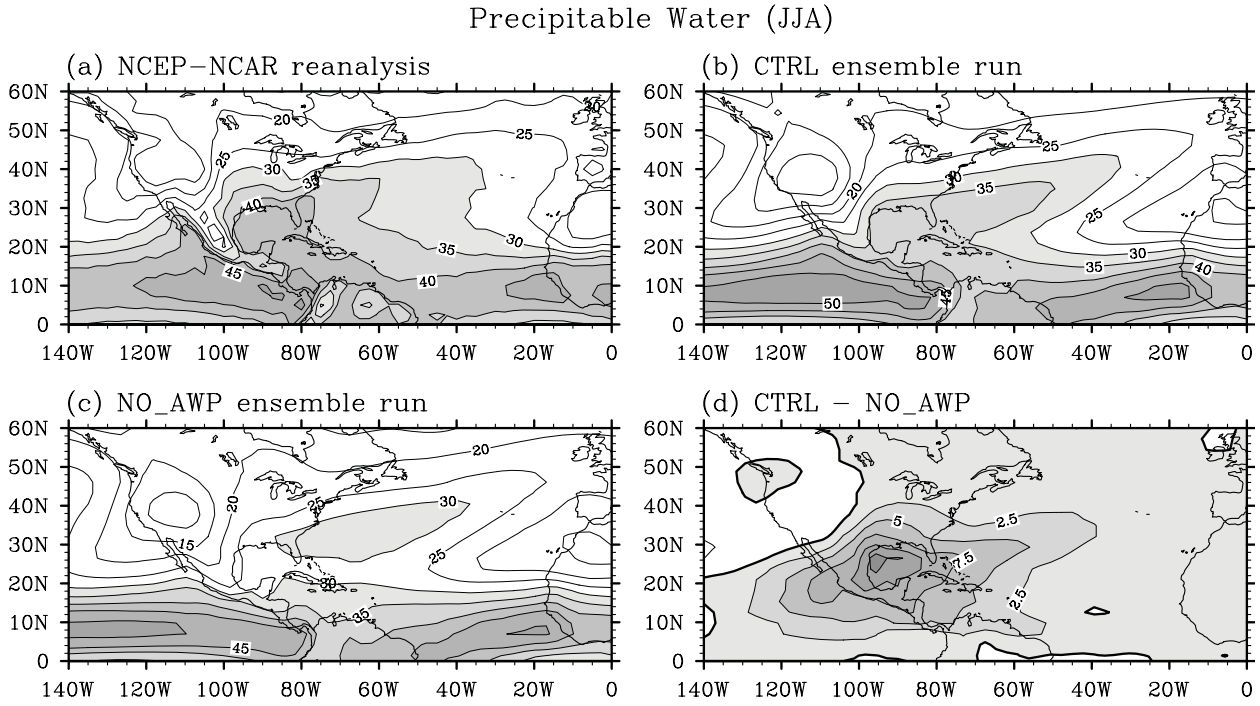

Figure 13. Summer (JJA) precipitable water content (kg m^{-2}) from (a) the NCEP-NCAR reanalysis, (b) the CTRL ensemble run, (c) the NO_AWP ensemble run, and (d) the difference between the CTRL and NO_AWP runs. In (a)-(c), the precipitable water content larger than 30 kg m^{-2} is shaded and the contour interval is 5 kg m^{-2}. In (d), the positive precipitable water difference is shaded and the contour interval is 2.5 kg m^{-2}.

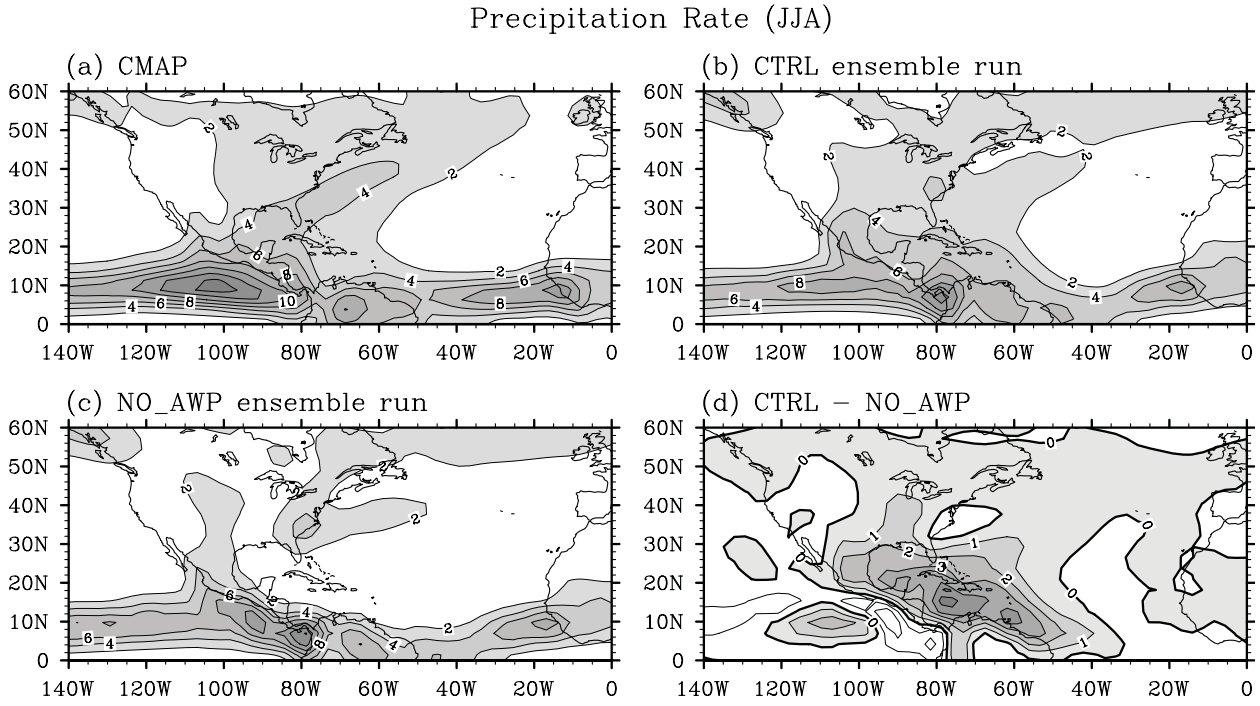

Figure 14. Summer (JJA) rainfall (mm day^{-1}) distribution from (a) the CMAP product, (b) the CTRL ensemble run, (c) the NO_AWP ensemble run, and (d) the difference between the CTRL and NO_AWP runs. In (a)-(c), the rainfall larger than 2.0 mm day^{-1} is shaded and the contour interval is 2 mm day^{-1}. In (d), the positive rainfall difference is shaded and the contour interval is 1.0 mm day^{-1}.

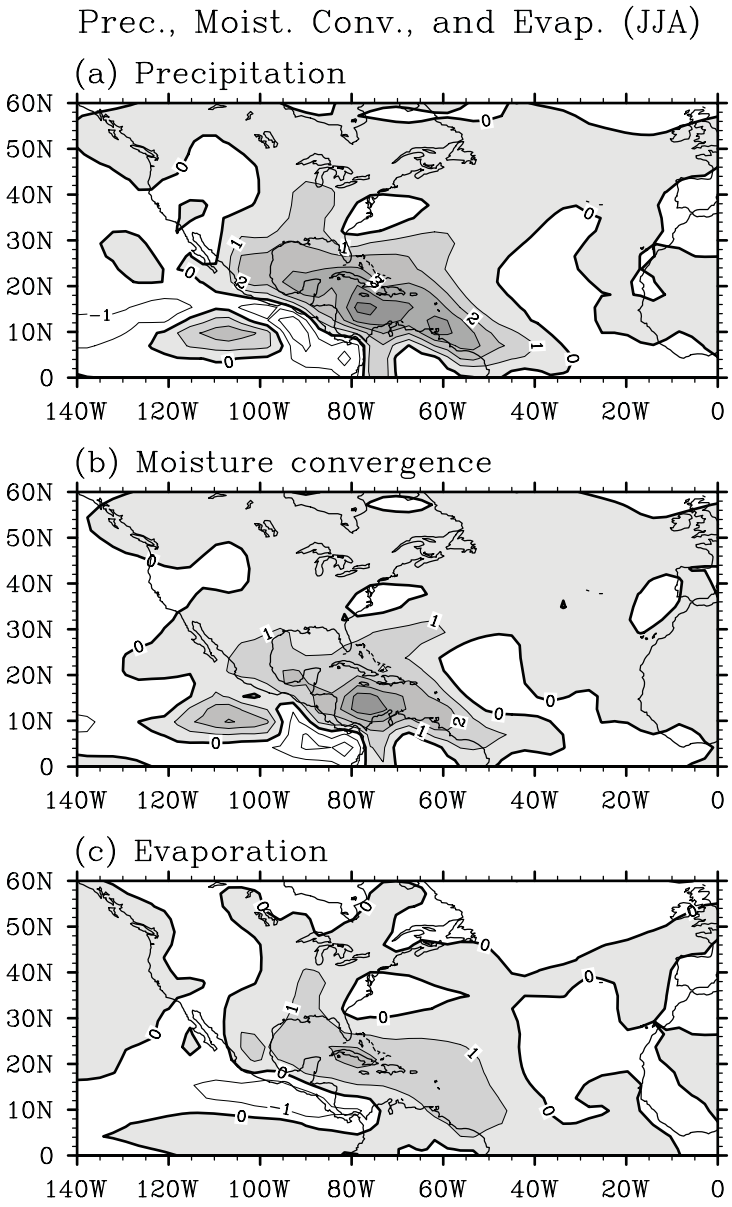

Figure 15. Precipitation, moisture convergence [$-\nabla \bullet \vec{Q}$, where $\vec{Q} = \int_{300\,mb}^{sfc} (q\vec{u} / g) dp$], and evaporation. Shown is the difference between the CTRL and NO_AWP runs for (a) precipitation (mm day^{-1}), (b) moisture convergence (mm day^{-1}), and (c) evaporation (mm day^{-1}). The positive value is shaded and the contour interval is 1.0 mm day^{-1}.

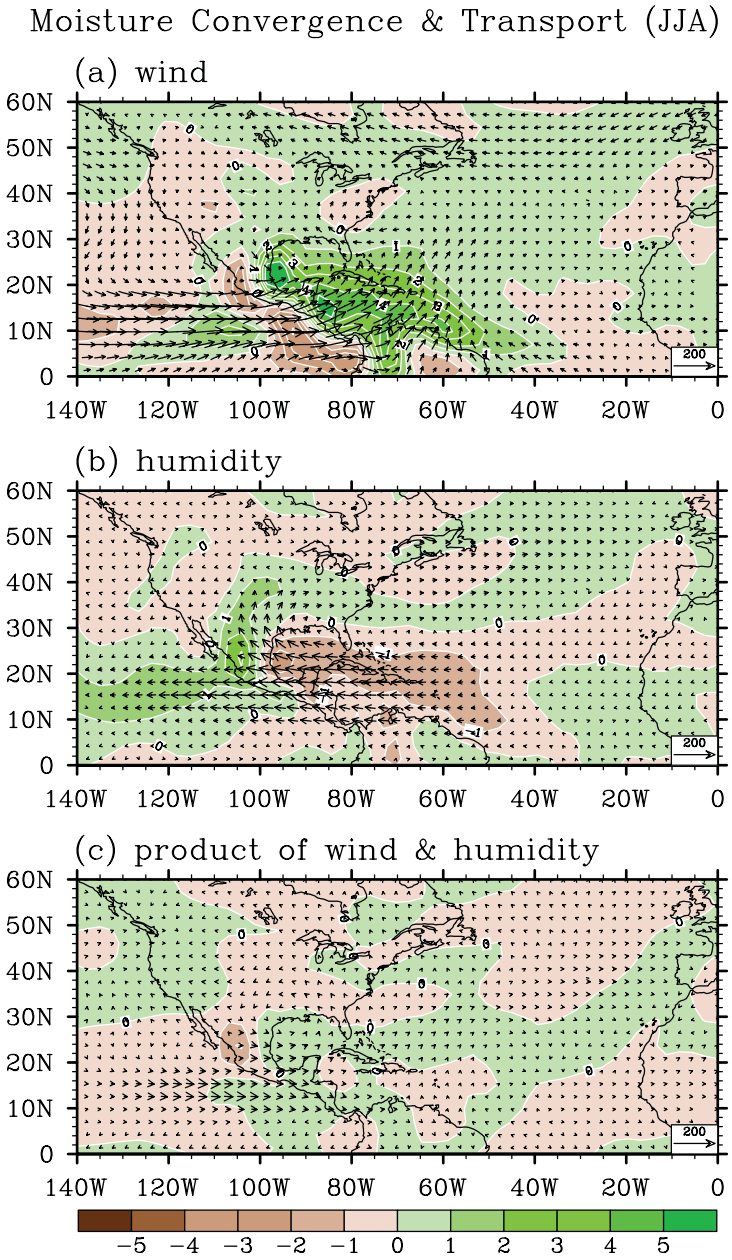

Figure 16. The moisture convergence (contour; mm day^{-1}) and transport (vector; kg m^{-1} s^{-1}) difference between the CTRL and NO_AWP runs during June-August (JJA) contributed by (a) the wind change $\left(-\nabla\bullet\left[\int_{300\,mb}^{sfc}(q\Delta\vec{u}/g)dp\right]\right.$ and $\left.\int_{300\,mb}^{sfc}(q\Delta\vec{u}/g)dp\right)$, (b) the specific humidity change $\left(-\nabla\bullet\left[\int_{300\,mb}^{sfc}(\vec{u}\Delta q/g)dp\right]\right.$ and $\left.\int_{300\,mb}^{sfc}(\vec{u}\Delta q/g)dp\right)$, and (c) the product of the wind and specific humidity changes $\left(-\nabla\bullet\left[\int_{300\,mb}^{sfc}(\Delta q\Delta\vec{u}/g)dp\right]\right.$ and $\left.\int_{300\,mb}^{sfc}(\Delta q\Delta\vec{u}/g)dp\right)$. $\Delta\vec{u}$ (Δq) represents the wind vector (specific humidity) difference between the CTRL and NO_AWP runs.

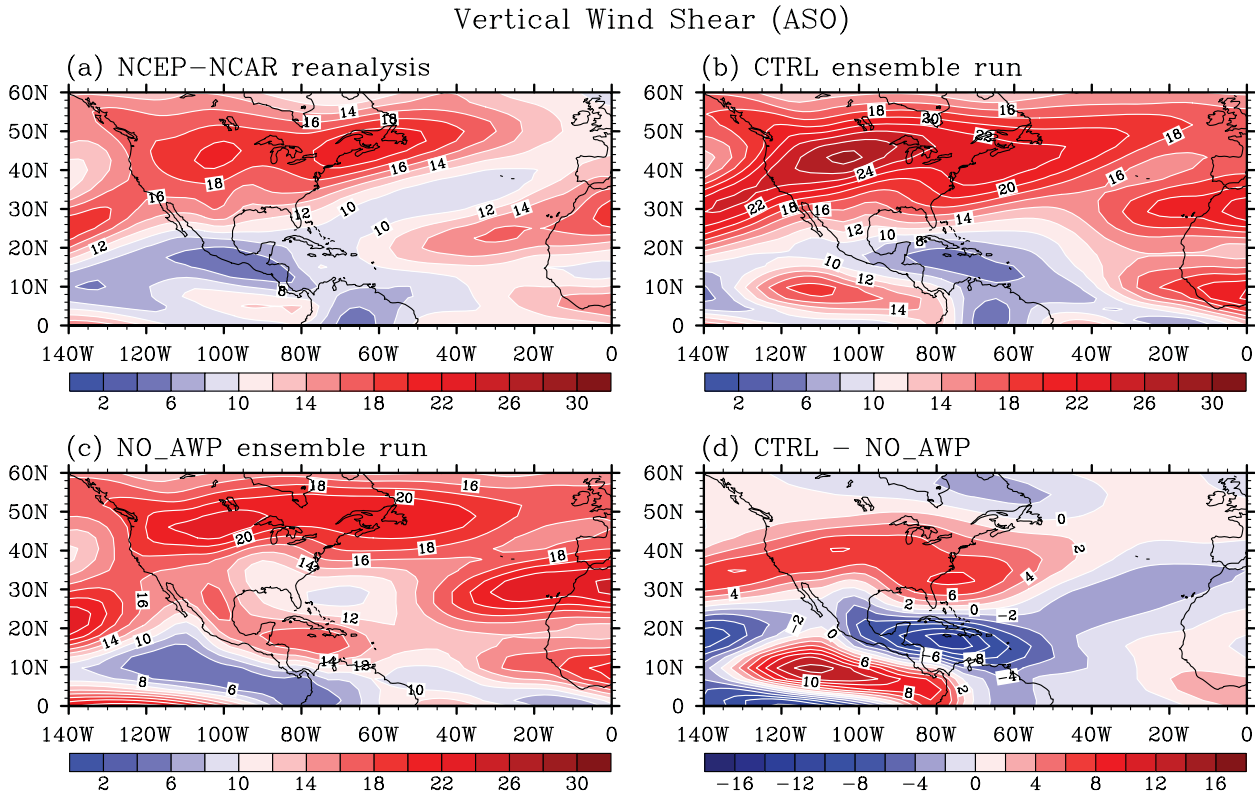

Figure 17. Tropospheric vertical wind shear ($\left[(U_{200}-U_{850})^2+(V_{200}-V_{850})^2\right]^{1/2}$; m s^{-1}) during August-October (ASO) from (a) the NCEP-NCAR reanalysis, (b) the CTRL ensemble run, (c) the NO_AWP ensemble run, and (d) the difference between the CTRL and NO_AWP runs.

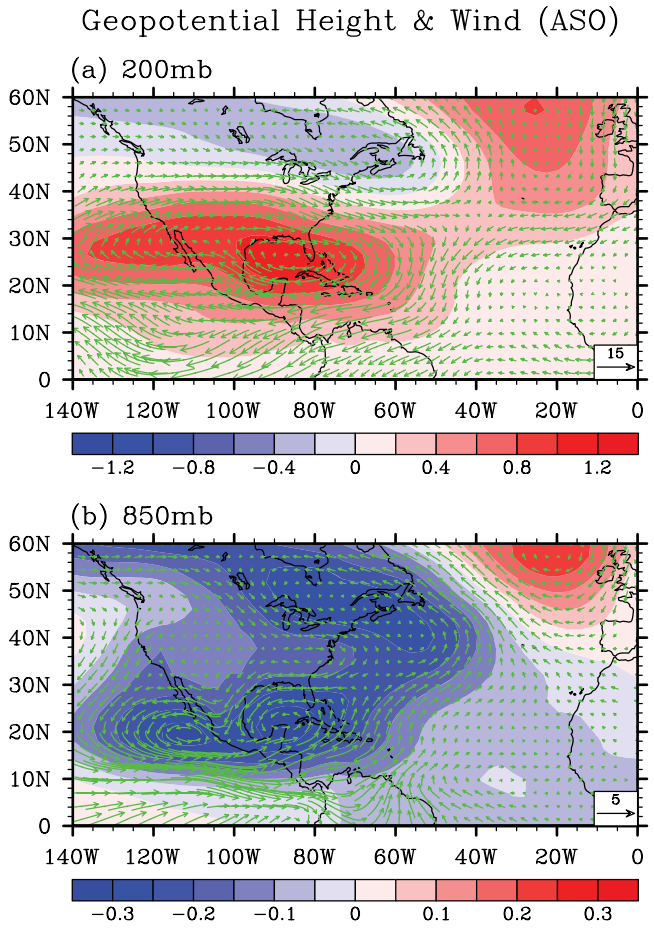

Figure 18. Geopotential height (10^2 m) and wind (m s^{-1}) difference between the CTRL and NO_AWP runs during August-October (ASO) at (a) 200-mb and (b) 850-mb.